

## RESEARCH ARTICLE

[View Article Online](#)  
[View Journal](#)

Cite this: DOI: 10.1039/c8md00095f

## Effect of N-1 arylation of monastrol on kinesin Eg5 inhibition in glioma cell lines†

Itamar Luís Gonçalves,<sup>a</sup> Lilia Rockenbach,<sup>‡a</sup> Gustavo Machado das Neves,<sup>a</sup> Gabriela Göethel,<sup>b</sup> Fabiana Nascimento,<sup>a</sup> Luciano Porto Kagami,<sup>a</sup> Fabrício Figueiró,<sup>c</sup> Gabriel Oliveira de Azambuja,<sup>a</sup> Amanda de Fraga Dias,<sup>c</sup> Andressa Amaro,<sup>c</sup> Lauro Mera de Souza,<sup>d</sup> Ivan da Rocha Pitta,<sup>e</sup> Daiana Silva Avila,<sup>f</sup> Daniel Fábio Kawano,<sup>g</sup> Solange Cristina Garcia,<sup>b</sup> Ana Maria Oliveira Battastini<sup>c</sup> and Vera Lucia Eifler-Lima<sup>\*,a</sup>

An original and focused library of two sets of dihydropyrimidin-2-thiones (DHPMs) substituted with N-1 aryl groups derived from monastrol was designed and synthesized in order to discover a more effective Eg5 ligand than the template. Based on molecular docking studies, four ligands were selected to perform pharmacological investigations against two glioma cell lines. The results led to the discovery of two original compounds, called **20h** and **20e**, with an anti-proliferative effects, achieving IC<sub>50</sub> values of about half that of the IC<sub>50</sub> of monastrol in both cell lines. As with monastrol, flow cytometry analyses showed that the **20e** and **20h** compounds induced cell cycle arrest in the G<sub>2</sub>/M phase, and immunocytochemistry essays revealed the formation of monopolar spindles due to Eg5 inhibition without any toxicity to *Caenorhabditis elegans*.

Received 19th February 2018,  
Accepted 14th April 2018

DOI: 10.1039/c8md00095f

[rsc.li/medchemcomm](http://rsc.li/medchemcomm)

## Introduction

Gliomas are the most common primary cancer in the central nervous system.<sup>1</sup> Glioblastoma multiform is considered the most aggressive and lethal form of glioma, with a patient survival rate limited to a few months.<sup>2</sup> This context has been observed even through the adoption of current therapeutic protocols, which involve a combination of surgery, radiotherapy and chemotherapy. Chemotherapy is usually performed worldwide with the pro-drug temozolomide, an orally admin-

istered alkylating agent that reaches the central nervous system in therapeutic concentrations.<sup>3</sup>

The search for new anti-glioblastoma agents still represents a great challenge, mainly due to the many malignant characteristics of glioblastoma multiform,<sup>4</sup> such as: a) undefined cell infiltration boundaries to adjacent healthy tissue, which hinders complete surgical removal; b) multiple mechanisms of drug resistance; c) the presence of areas of hypoxia with inactive mitotic cells; d) the cancer stem cell populations; and e) the presence of a blood-brain barrier, which limits the bioavailability of drugs to the brain.<sup>5</sup> In addition to these factors, a major challenge for the discovery of new drugs for the treatment of cancer is finding molecules that have good levels of tolerability and pharmacokinetic profiles, and produce minimal adverse effects; they must also show efficacy in curing the disease or significantly increase the patients' survival rate.

One of the most explored targets for anticancer drug design is mitotic cell division, a complex process that is of crucial importance for cellular proliferation and tumor growth. Mitotic inhibitors currently used as antitumor drugs include taxanes and vinca alkaloids, such as paclitaxel, vincristine, vinblastine and colchicine. These compounds affect the polymerization of microtubules by binding to tubulin. When exerting activity directly on tubulin, these drugs affect different cellular functions that are dependent on microtubule activity, such as cell mobility, the transport of organelles and

<sup>a</sup> Laboratório de Síntese Orgânica Medicinal/LaSOM, Faculdade de Farmácia, Universidade Federal do Rio Grande do Sul, Avenida Ipiranga, 2752, Porto Alegre/RS, Brazil. E-mail: veraeifler@ufrgs.br

<sup>b</sup> Laboratório de Toxicologia – LATOX, Faculdade de Farmácia, Universidade Federal do Rio Grande do Sul, Porto Alegre/RS, Brazil

<sup>c</sup> Departamento de Bioquímica, ICBS, Universidade Federal do Rio Grande do Sul, Porto Alegre/RS, Brazil. E-mail: abattastini@gmail.com

<sup>d</sup> Instituto de Pesquisa Pelé Pequeno Príncipe, Faculdades Pequeno Príncipe, Curitiba-PR, Brazil

<sup>e</sup> Núcleo de Pesquisa em Inovação Terapêutica, Universidade Federal de Pernambuco, Recife/PE, Brazil

<sup>f</sup> Grupo de Pesquisa em Bioquímica e Toxicologia em *Caenorhabditis elegans* (GBToxCE), Universidade Federal do Pampa-UNIPAMPA, Uruguaiana, RS, Brazil

<sup>g</sup> Faculdade de Ciências Farmacêuticas, Universidade Estadual de Campinas, Campinas-SP, Brazil

† Electronic supplementary information (ESI) available. See DOI: 10.1039/c8md00095f

‡ These authors have contributed equally to this work.

vesicles<sup>6</sup> and neuro-transportation; consequently, they trigger side effects, such as peripheral neuropathy.<sup>7</sup> Another way to affect microtubule dynamics in cell division is the inhibition of kinesin Eg5, a mitosis motor protein that regulates spindle elongation at prophase; this contributes to centrosome separation, through which genetic material moves to the poles of the cell during metaphase. Inhibition of Eg5 produces disruption of the cell cycle in the G<sub>2</sub>/M phase and consequent cell death by apoptosis.<sup>8</sup> Therapeutic use of Eg5 inhibitors has the potential of overcoming the resistance of neoplastic tissue against drugs targeting the polymerization of microtubules.<sup>9</sup> Furthermore, Eg5 expression in non-proliferating adult tissue is generally negligible; meanwhile, in neoplastic tissue, Eg5 is highly expressed and related to aggressiveness and lack of response to chemotherapy.<sup>10</sup> Kinesin Eg5 is overexpressed in many kinds of tumors, such as breast carcinogenesis,<sup>11</sup> laryngeal squamous cell carcinoma,<sup>12</sup> astrocytic neoplasm,<sup>13</sup> prostate cancer,<sup>14</sup> bladder cancer<sup>15</sup> and renal cell carcinoma.<sup>8</sup> Thus, inhibition of Eg5 increases selectivity over mitotically active cells<sup>16</sup> and cancer cells,<sup>8,11–15</sup> which results in fewer side effects and greater effectiveness; therefore, Eg5 is a promising anticancer target.

Monastrol 1 (Fig. 1) is responsible for the discovery of Eg5 as a new target for cancer treatment; it was identified in 1999 as the first small molecule to present targeted Eg5 inhibition. Monastrol 1 received this name because it induces the formation of a single mitotic spindle, replacing the bipolar spindles that are characteristic of cell division.<sup>17</sup> Evidence supports that monastrol 1 effects allosteric inhibition of Eg5, leading to a conformational change that prevents the release of ADP from the protein in the ADP-Eg5 complex. The active site of Eg5, therefore, remains occupied, preventing the binding of a new molecule of ATP.<sup>18</sup>

Based on this fact, since the identification of the role of monastrol 1 in Eg5 inhibition, a variety of dihydropyrimidin-2-thiones (DHPMs) have been obtained with the aim of developing more potent compounds (Fig. 1). Since 2005, many researchers have been dedicated to searching for new dihydropyrimidin-2-thiones with antitumor activity; these are currently considered to be privileged structures due to the diverse pharmacological activities found for this class of compounds.<sup>19,20</sup> Monastrol 1 produced moderate allosteric inhibition in Eg5, while its analogue *p*-monastrol 2 presented insignificant effects on Eg5.<sup>18</sup> In 2005 it was reported that enastrol 3, enastron 4 and dimethylenastron 5 present greater inhibition activity on Eg5 than monastrol.<sup>21</sup> Among the monastrol derivatives with low inhibitory capacity, it is also

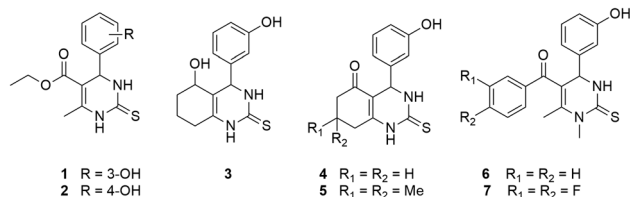


Fig. 1 Monastrol 1 and derivatives.

possible to highlight structures 6 and 7, identified as mon-97 and fluoroastrol.<sup>22</sup> Recently, various inhibitors of Eg5 have reached the clinical stage (Fig. 2, structures 8–13); however, there are no drugs on the market that act on Eg5.<sup>10</sup>

Previous results obtained in our laboratory have shown that DHPMs can inhibit the growth of glioma cancer cells.<sup>23–25</sup> In this current work, molecular modeling was employed to elucidate the possible interactions of DHPMs with the active site of Eg5, such as a hydrophobic pocket near the N-1 position. With the aim of verifying this possibility and, consequently, the effects of arylation on these interactions, a focused library of new dihydropyrimidin-2-thiones (DHPMs) were synthesized and their activities were evaluated.

## Results and discussion

### Chemistry

In recent years, many approaches to structural changes in DHPMs have focused on C-5 ester side chain modifications,<sup>26</sup> C-6 substitution changes<sup>27</sup> and, mainly, C-4 aromatic ring substitutions.<sup>26</sup> Few structural variations have been described in the literature related to the substitution of an aromatic ring in the N-1 position of the dihydropyrimidine nucleus; thus, most of the molecules obtained in the present work are novel. Once the DHPMs are built, the regioselectivity is high and the reactions occur on N-3 instead of the less reactive N-1. In fact, a few publications can be found wherein DHPM N-1 alkylation was achieved;<sup>28,29</sup> however, no publications describing arylation at N-1 of the DHPM have been found. For this purpose, it appears that the best strategy is to link the aromatic moiety to nitrogen 1 before the Biginelli reaction. Few studies in the literature using this strategy with the aim of functionalizing N-1 with an aryl group have been found,<sup>22,30–37</sup> and only one reports some pharmacological activity;<sup>32</sup> many of these approaches employed phenylthiourea, with limited substituents linked to the aromatic ring. There is potential for exploration of the development of routes for obtaining N-1 aryl-substituted dihydropyrimidin-2-thiones and prospecting their anticancer activities.

The two series of N-1-aryl-substituted dihydropyrimidin-2-thiones, 19a–k and 20a–k, were synthesized in three steps by a convergent approach where the N-1 substitution was added

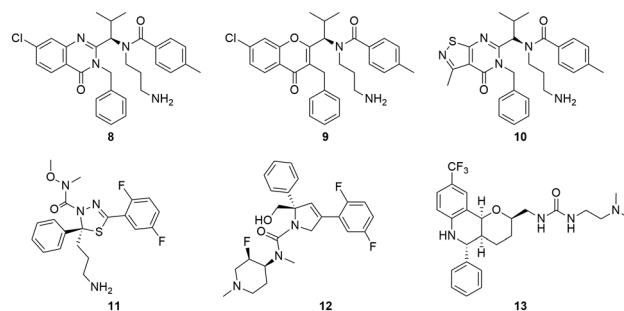


Fig. 2 Inhibitors of Eg5 in clinical stage investigations.

at the thiourea moiety in two steps followed by the Biginelli reaction in the last step (Scheme 1). In order to compare their pharmacological effects with monastrol **1**, the series **19a–k** has no substitution at the benzene ring; meanwhile, the other series, **20a–k**, contains an OH at C-3, like monastrol **1**. The eleven N-1 arylthioureas **16a–k** were obtained in two steps with high purity (Scheme 1), starting with the reaction of benzoyl chloride **14** with ammonium thiocyanate; this allows the isothiocyanate intermediate to react with anilines with different substituents to provide **15a–k**. Hydrolysis of these intermediates with NaOH led to the mono-substituted thioureas **16a–k**. With the exception of **16e** and **16f**, the intermediates obtained were used in consecutive steps without purification. The yield range was 40% to 82%.

With the thioureas **16a–k** in hand, the Biginelli reaction was accomplished using ethyl acetoacetate **18** and benzaldehyde **17a** or 3-hydroxybenzaldehyde **17b** as building blocks. The reactions were carried out in the presence of trimethylsilane chloride (TMSCl) as a promoting agent at room temperature for 72 hours. In all cases, the product precipitated quantitatively when the reactional medium was poured in the water. All the compounds were obtained with high purity and good yields, in accordance with the analytical data reported here and in the ESI†

This methodology enabled the rapid attainment of 22 dihydropyrimidin-2-thiones with various substitution patterns at N-1 using mild reaction conditions. The different substitution patterns at N-1 included aromatic rings exhibiting electron donor and acceptor substituents with different electronic effects on the ring (Table 1). In fact, the N-1 position in the dihydrothiopyrimidine core has been poorly explored; to the best of our knowledge, with the exception of compound **19a**, the chemical library generated here is original. Thus, this research represents an important contribution to the structural diversity of this class of molecules.

### Selection of compounds by molecular docking

The determination of the crystallographic structure of monastrol **1** and of different complex compounds with

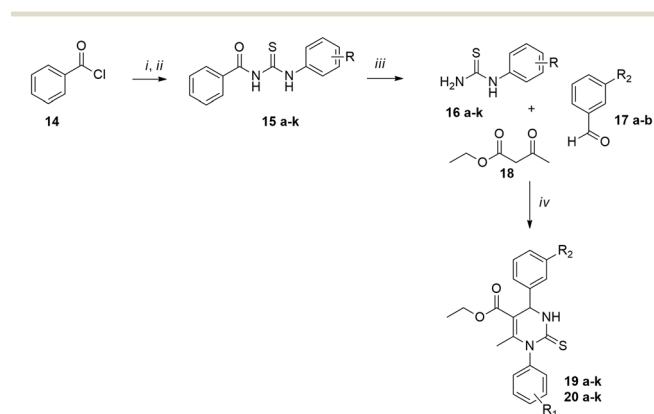
kinesin Eg5 offered important information for the development of new ligands for this protein. The allosteric binding site of Eg5 has been further studied through molecular modeling techniques and has been found to contain three hydrophobic subpockets (P1–P3) which interact with the inhibitors.<sup>38,39</sup> Analysis of the crystallographic pose of monastrol within Eg5 demonstrated that the insertion of an aromatic ring with a different pattern of substitution in the N-1 nitrogen of the dihydropyrimidine nucleus may lead to improvement in the interaction of dihydropyrimidin-2-thiones with Eg5. These modifications may promote better interaction of the ligand with Eg5 by the site identified as the hydrophobic subpocket 3 (P3 in Fig. 3). Considering these findings, 2 series of compounds with aromatic substituents at N-1 were designed, and a virtual screening at the kinesin Eg5 crystallographic complex (PDB ID: 1X88) was performed.

The validation step was performed through both re-docking and cross-docking procedures by using eight distinct crystallographic ligands. The results show that these parameters are suitable for the vast majority of ligands, including other DHPM derivatives and a trityl-cysteine, containing at least one pose with a RMSD value fulfilling the adopted criteria. The docking parameters, however, did not achieve the arrangement of large compounds, such as ispinesib, showing poses with RMSD equal to or higher than 4.0 Å (Table S1 in the ESI†).

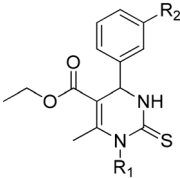
The cross-docking procedure may be considered a more difficult task if compared to re-docking, showing a 20% decrease in success rate.<sup>40</sup> Moreover, the ability of docking programs to fit a ligand into a non-native protein conformer is lower when the ligand possesses a very large structural difference in comparison with the native protein.<sup>41</sup> Although high RMSD values were observed for the large ligands, the obtained results suggest high accuracy of the established parameters for both the re-docking and cross-docking procedures, especially for ligands that are structurally similar to monastrol **1**.

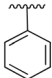
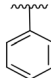
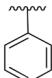
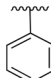
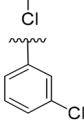
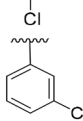
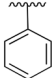
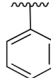
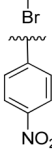
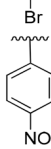
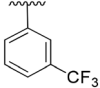
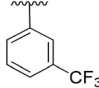
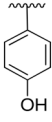
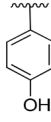
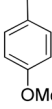
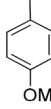
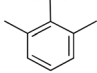
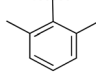
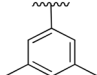
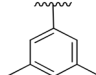
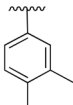
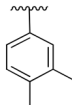
The virtual screening of the designed DHPMs revealed that the two best compounds, which displayed acceptable poses and had high GoldScore values, showed ranks better than monastrol **1** (Table 2). These compounds, **20e** and **19h**, and their counterpart analogues **19e** and **20h** were then chosen for further analyses in order to predict their interactions with the kinesin binding site compared to the superposed crystallographic ligands, monastrol and fluorastrol. Moreover, the ligands were evaluated according to their capacity for exploring the aimed hydrophobic subpocket P3.

The compounds **20e** and **19e** displayed similar binding modes with strong resemblance to the crystallographic pose of monastrol **1**, especially at their aromatic moieties, 4-(3-hydroxyphenyl) and 4-phenyl, respectively; these may interact with the subpocket P2 through hydrophobic interactions with Gly117, Glu118, Arg119, Ala133 and Pro137. The 4-(3-hydroxyphenyl) group from **20e** may further interact with Glu118 through hydrogen bonds, whereas this interaction may not be observed in **19e** due to the lack of the hydroxyl function. The N1 substituent of both compounds, a 4-nitro-



**Scheme 1** (i)  $\text{NH}_4\text{SCN}$ , acetone, reflux, 15 min; (ii)  $\text{PhNH}_2$ , acetone, reflux, 30 min. (iii) NaOH 5% to 10%, 10 to 30 min, 90 °C; (iv) TMSCl, DMF, 1 h ultrasound, r.t. 72 h.

**Table 1** Structures of the as-synthesized compounds


Compound	R <sub>1</sub>	R <sub>2</sub>	Compound	R <sub>1</sub>	R <sub>2</sub>
19a		H	20a		OH
19b		H	20b		OH
19c		H	20c		OH
19d		H	20d		OH
19e		H	20e		OH
19f		H	20f		OH
19g		H	20g		OH
19h		H	20h		OH
19i		H	20i		OH
19j		H	20j		OH
19k		H	20k		OH

phenyl group, may explore the subpocket P3 through hydrophobic interactions with Leu160, Leu214, Gly217, Ala218 and Arg221, through hydrogen bonds with Glu116, and through an anion- $\pi$  interaction between the side chain of Glu116 and the aromatic ring (Fig. 4 and Tables S2–S4 in the ESI†). The most crucial difference observed between these two molecules relies on the 3-hydroxyl group of the phenyl moiety, which may interact through hydrogen bonds with the main chain carbonyl group of Glu118 and which is absent in 19e.

The importance of the 3-hydroxyl feature in monastrol derivatives was previously characterized through comparison of both class I inhibitors (monastrol, enastron and dimethylenastron) and class II inhibitors (mon-97 and fluorastrol), which contain this group as a common moiety; therefore, it may be concluded that the 3-hydroxyl feature is essential for the activity of the molecule.<sup>42</sup>

The second pair of analogue compounds, 19h and 20h, assumed binding modes similar to the crystallographic pose of

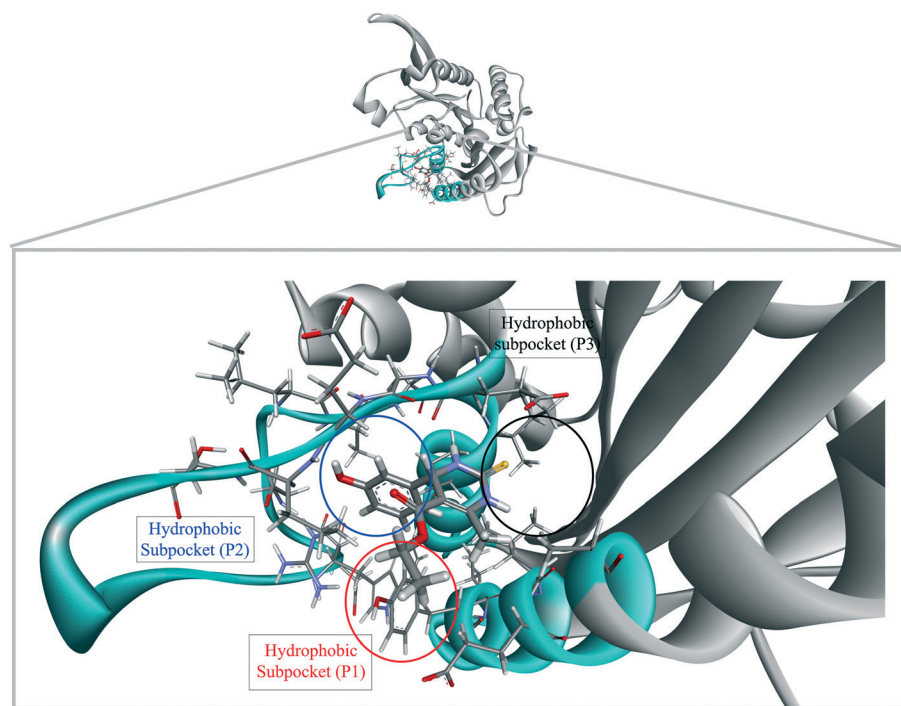


**Fig. 3** Crystallographic complex of monastrol **1** with the allosteric binding site of kinesin Eg5 (PDB ID: 1X88) showing the three hydrophobic subpockets: P1 (red), P2 (blue) and P3 (black).

fluorastrol **13**, with the thione moiety pointing out towards the surface and the aromatic components, 4-(3-hydroxy-phenyl) and 4-phenyl, occupying the P2 subpocket. They may interact with the following common residues: Glu118, Arg119, Ala133 and Tyr211. Additionally, **19h** may further interact with the main chain carboxyl oxygen from Gly117 and with the main chain amine group from Arg119. The observed difference in the pose orientation of both compounds led to a considerable change in the N-1 substituent, which

may interact with the P1 subpocket through Tyr211, Glu215, Ala218 and Ala219, assuming the same position as the *N*-methyl group from fluorastrol; however, the *N*-methyl group does not appear to interact with the binding site. The ester moiety of **19h** and **20h** may interact with both P2 and P3 through hydrophobic contacts with Glu116, Ile136, Pro137 and Leu214 (Fig. 5 and Tables S5–S7 in the ESI†).

The two best compounds from both series (**19e**, **20e**, **19h** and **20h**) were selected by the docking procedure. It was shown that these compounds may interact with the kinesin Eg5 binding site in at least two poses, assuming the monastrol configuration or the fluorastrol configuration. This finding is in agreement with that related by Prokopcová and co-workers, in which the authors found that the docked compounds may only adopt two docking poses related to class I and class II DHPM analogues.<sup>22</sup> The four compounds were also investigated according to their predicted binding affinities using X-Score and were compared to monastrol **1**. The predicted values for all the four compounds were higher than those predicted for monastrol **1** (Table 3). These results suggest that the evaluated compounds may bind with greater affinity to the binding site than monastrol.

### Antitumor activity

**Cell viability.** With the aim of verifying the anticancer activity of the monastrol derivatives selected by molecular docking, cell viability was analyzed by MTS assay after treatment with 5, 10, 25, 50 and 100  $\mu$ M of monastrol **1** or its derivatives **19e**, **20e**, **19h** and **20h** for 24 hours. As can be observed in Fig. 6, **19h**, **20e** and **20h** showed better profiles of

**Table 2** Virtual screening ranking of the designed DHPMs and the crystallographic ligands based on their best poses according to their GoldScore values. The ligands, shown in bold, were selected with their counterparts for further binding mode analyses. The ligands are represented according to their PDB ligand codes: monastrol (NAT); enastron (KZ9); dimethylenastron (EGB); fluorastrol (X7E); *S*-trityl-L-cysteine analogue (V02); triphenylbutanamine analogue (DQ6); Sb743921 (6LX); ispinesib (G7X)

Structure	GoldScore	Rank	Structure	GoldScore	Rank
6LX	81.8666	1	<b>19c</b>	59.3787	16
V02	73.3863	2	<b>20a</b>	58.8010	17
DQ6	69.8569	3	<b>20h</b>	58.6443	18
G7X	67.2378	4	<b>20b</b>	58.1574	19
<b>20e</b>	66.5438	5	<b>19i</b>	56.9552	20
X7E	65.0821	6	<b>20j</b>	56.5571	21
<b>19e</b>	63.5348	7	<b>20i</b>	54.9600	22
<b>20g</b>	62.7548	8	<b>20f</b>	54.8859	23
<b>19h</b>	62.2357	9	<b>20k</b>	53.9910	24
NAT	60.8637	10	<b>19k</b>	52.4179	25
<b>19g</b>	60.6676	11	<b>19f</b>	52.3876	26
EGB	60.6326	12	<b>20d</b>	50.0315	27
<b>20c</b>	60.5947	13	<b>19j</b>	49.6185	28
KZ9	60.5311	14	<b>19b</b>	49.5652	29
<b>19a</b>	59.7063	15	<b>19d</b>	47.4533	30



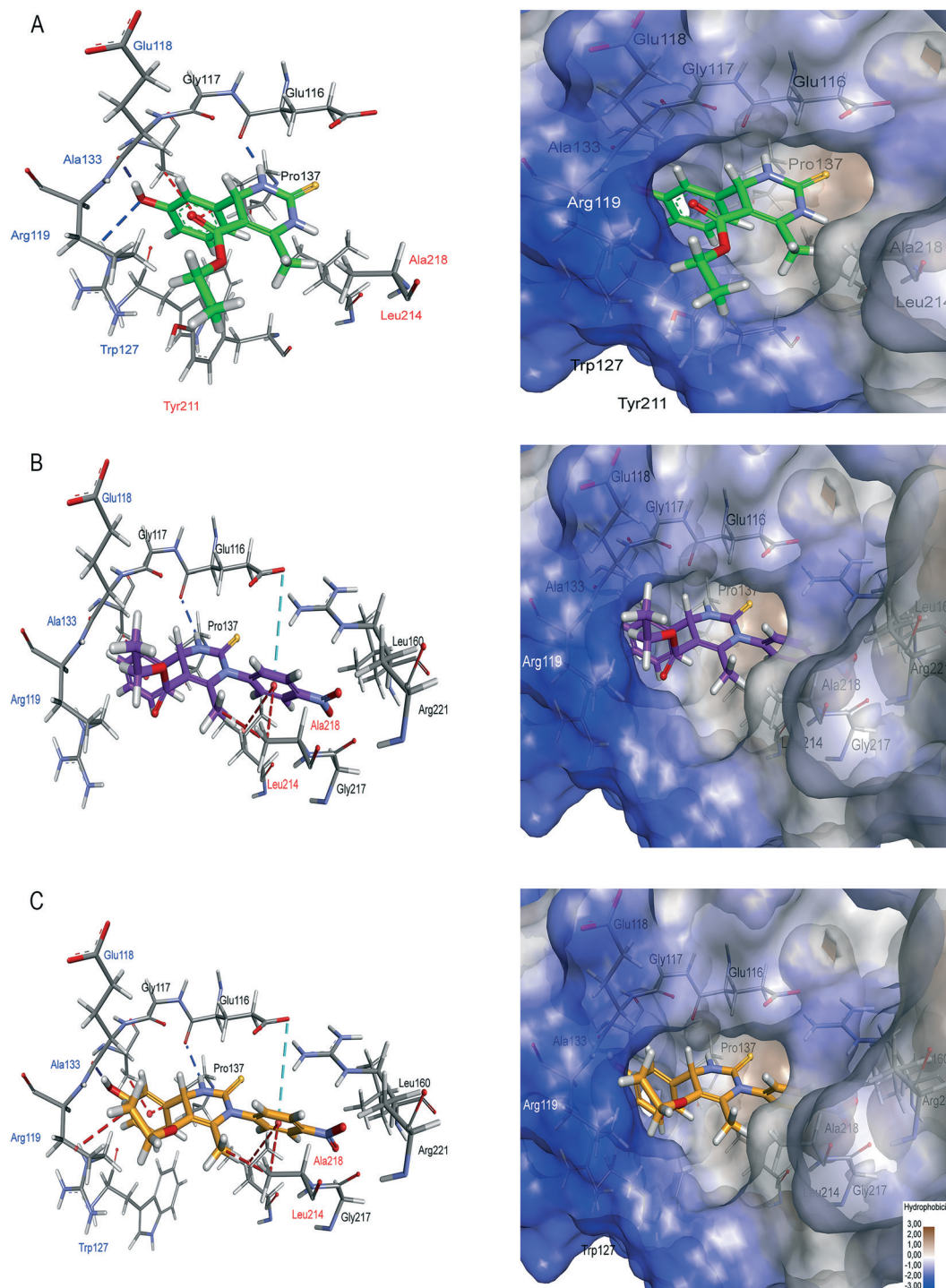


**Fig. 4** (Left) The allosteric binding site of kinesin Eg5 (PDB ID: 1X88) illustrating the interactions with the crystallographic pose of monastrol **1** (A) and the best docked poses of **19e** (B) and **20e** (C). The interactions are represented as dashed lines in the following colors: hydrogen bonds (dark blue), hydrophobic interactions (red) and anion- $\pi$  (cyan). The binding pocket amino acids were labeled with different colors to represent their associations with a specific subpocket: P1 (red); P2 (blue); P3 (black). (right) Solid surface representations of the kinesin Eg5 binding site and the respective ligands, indicating the hydrophobicity of the binding pocket.

anti-proliferative activity than monastrol **1** in both glioma cell lines. In the human cell line U138 (Fig. 6A), 100  $\mu$ M of monastrol **1** decreased  $20.8 \pm 2.99\%$  while, the derivatives **20e**, **19h** and **20h** decreased approximately 2-fold in comparison with monastrol cell viability in the U138 glioma cells

( $45.6 \pm 3.24\%$ ,  $40.2 \pm 4.84\%$  and  $40.8 \pm 5.27\%$ , respectively). Similar results were obtained with the C6 rat glioma cell line, where the three N-1-aryl DHPMs, **20e**, **19h** and **20h**, were shown to be more cytotoxic than monastrol **1** (Fig. 6B). However, in this case, **20e** and **20h** were more effective than **19h**

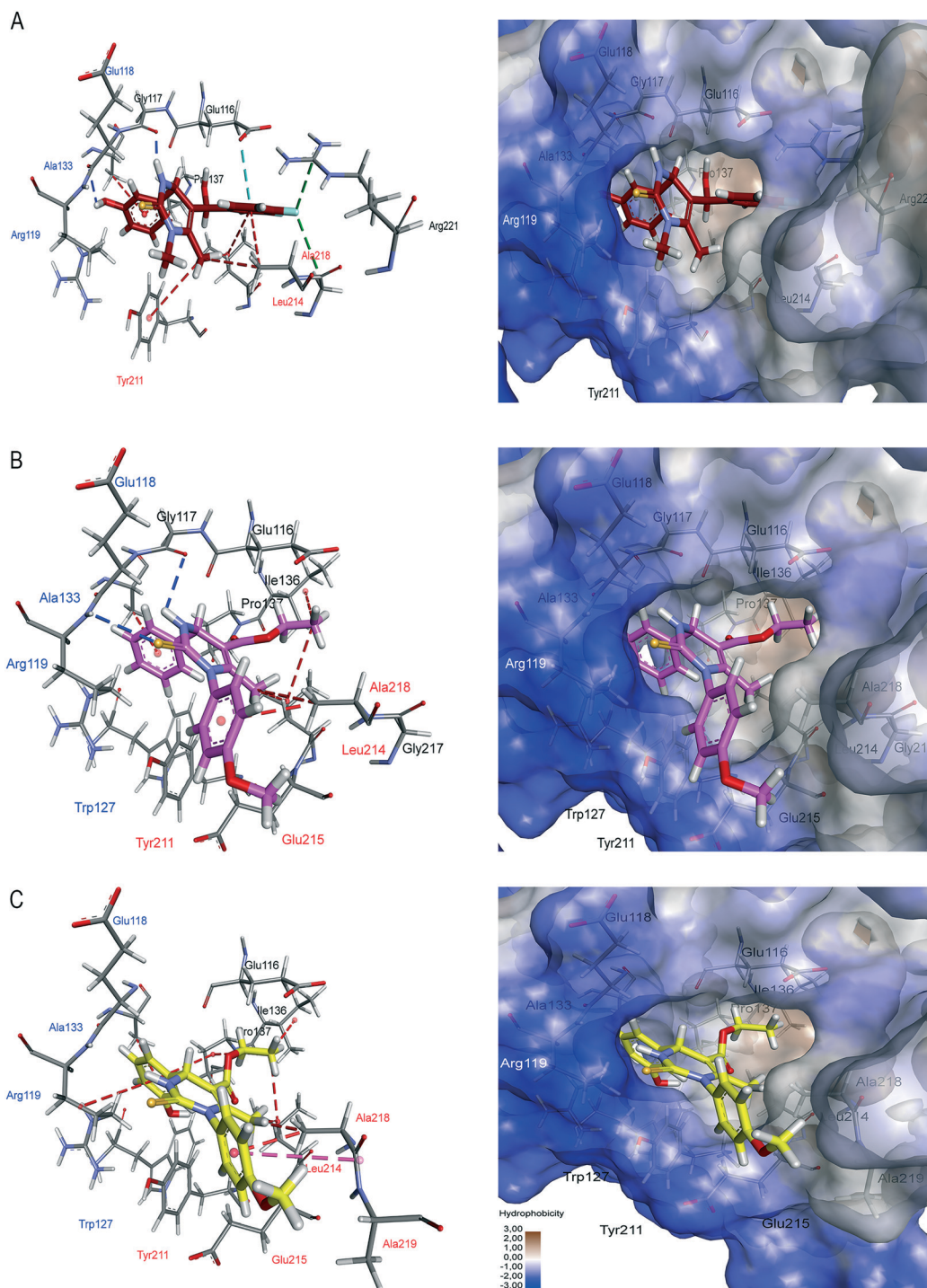


**Fig. 5** (Left) The allosteric binding site of kinesin Eg5 (PDB ID: 1X88) illustrating the interactions with the superposed crystallographic fluorastrol (A) and the best docked poses of **19h** (B) and **20h** (C). The interactions are represented as dashed lines in the following colors: hydrogen bonds (dark blue); hydrophobic interactions (red); anion- $\pi$  (cyan); amide- $\pi$  stacking (pink); and halogen interactions (dark green). The binding pocket amino acids were labeled with different colors to represent their associations with a specific subpocket: P1 (red); P2 (blue); P3 (black). (right) Solid surface representations of the kinesin Eg5 binding site and the respective ligands, indicating the hydrophobicity of the binding pocket.

in decreasing the viability of C6 glioma cells ( $84.4 \pm 0.55\%$ ,  $79.4 \pm 8.15\%$  and  $51.6 \pm 4.39\%$ , respectively, at  $100 \mu\text{M}$ ).

The  $\text{IC}_{50}$  values of these five DHPMs in glioma cell lines U138 and C6 were calculated and are depicted in Table 4. In both cell lines, compounds **20e**, **19h** and **20h** reached  $\text{IC}_{50}$

values lower than half the  $\text{IC}_{50}$  of monastrol **1**. Derivatives **20e**, **19h** and **20h** showed greater cytotoxic effects against the C6 rat cell line than against the U138 human cell line; this probably occurred because C6 cells have a higher proliferative rate than U138 cells.



**Table 3** Predicted binding affinity values for the four compounds compared to monastrol (NAT) calculated by X-Score

Structure	GoldScore	X-Score	Binding energy
20e	66.5438	6.64	-9.06
19e	63.5348	6.56	-8.94
19h	62.2357	6.39	-8.72
20h	58.6443	6.20	-8.46
NAT	60.8637	6.02	-8.22

**Table 4** The IC<sub>50</sub> values of each compound for glioma cell lines U138 and C6

Molecule	U138 IC <sub>50</sub> (μM)	C6 IC <sub>50</sub> (μM)
Monastrol 1	>200	>200
19e	>200	>200
20e	114.1	54.7
19h	131.1	78.3
20h	142.7	57.1

This first result of N-1-aryl DHPMs against glioma cell lines endorses the importance of the 3-hydroxyl group of the phenyl moiety (R2), which may interact through hydrogen bonds with the main chain carbonyl group of Glu118 of Eg5, as this group is the only difference between 19e and 20e.

**Cell cycle and cell death.** Following the cell viability assays, where two compounds, 20e and 20h, displayed better inhibition against both glioma cell lines (U138 and C6) than the template 1, cell cycle and cell death analyses were performed to confirm the profile and the possible mechanism of cell viability decrease through Eg5 inhibition. The cells were treated with the IC<sub>50</sub> concentrations of the molecules; U138 was treated with 200 μM monastrol 1 or 150 μM of 20e or 20h, while C6 was treated with 100 μM monastrol 1 or 50 μM of 20e or 20h for 24 h to analyze the cell cycle and for 48 h to analyze cell death. As expected, and confirming the profile of Eg5 inhibitors, the treatments with 20e and 20h induced cell cycle arrest in the G<sub>2</sub>/M phase (Fig. 7A). Monastrol 1 increased G<sub>2</sub>/M cells at  $27.4 \pm 6.99$ ; 20e increased to  $8.7 \pm 2.68$  and 20h to  $10.4 \pm 1.68$ . The N-1-aryl DHPMs

showed a similar profile of monastrol 1 on cell cycle arrest in the U138 human cell line but not in the C6 rat cell line, where a lower extent of arrest in G<sub>2</sub>/M phase was induced by the synthesized compounds 20e and 20h in relation to monastrol 1. This may have occurred as a consequence of a combination of more potent inhibition of Eg5 by 20e and 20h and the doubling of the C6 population within 24 h, which culminated in faster cell death in C6 in comparison with the U138 cells, leading to cell death following cell cycle arrest before 24 h of analysis; it may also have occurred because in C6 cells, these compounds act by more than one mechanism.

As can be observed in Fig. 7B, 20e induced higher levels of apoptosis and necrosis than monastrol 1 in U138; meanwhile, in C6, monastrol 1 and 20h induced higher levels of apoptosis. Observing the cell cycle and cell death analyses, it is possible to note that 20h showed similar behavior in both cell lines, with a similar profile to that of the Eg5 inhibitor monastrol 1; however, this behavior was obtained with a smaller IC<sub>50</sub> concentration.

The above results identify the importance of the 3-hydroxyl group of the phenyl moiety and are in agreement with the molecular docking studies. Moreover, the insertion of an aromatic ring with a different pattern of substitution in the N-1 nitrogen of the dihydropyrimidin-2-thiones nucleus may lead to improvement in the activity against Eg5 by extending the interactions of the ligand within the binding site, especially with the hydrophobic subpocket 3 (P3) in Fig. 3. The potential of these two molecules is the first step for drug design for further *in vivo* tests.

**Immunocytochemistry.** Immunocytochemistry was performed by immunofluorescence to analyze the Eg5 inhibition of 1, 20e and 20h. The formation of monopolar spindles due to Eg5 inhibition was observed when the cells were treated with monastrol 1. Fig. 8B and F show the formation of monopolar spindles due to Eg5 inhibition; as expected, the N-1 aryl derivatives, 20e and 20h, present the same outcomes. Fig. 8C, D, G and H show the formation of monopolar spindles triggered by 20e and 20h, respectively. These immunofluorescence assay results are in agreement with those observed in the cell cycle and cell death analyses, where interruption of mitosis was observed by cell cycle arrest in the G<sub>2</sub>/M phase and apoptosis induction for both tested compounds. Therefore, these results indicate that 20e and 20h are Eg5 kinesin inhibitors and new anti-glioma drug candidates with greater potential than monastrol.

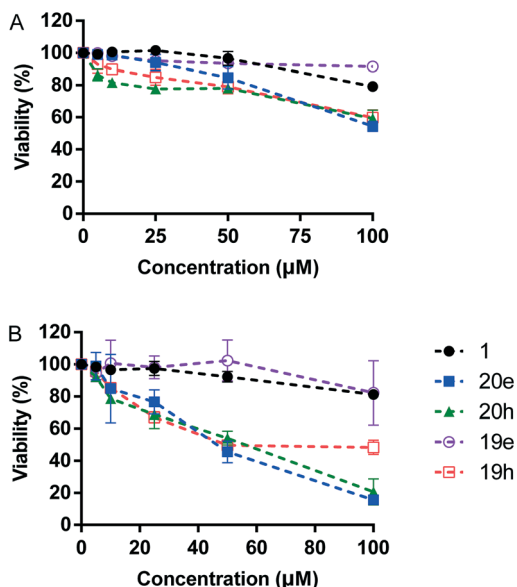


**Fig. 6** Cell viability: U138 (A) and C6 (B) cells were treated with monastrol 1 or N-1-aryl DHPMs 19e, 20e, 19h and 20h at 5, 10, 25, 50 and 100 μM for 24 h prior to the MTS assay. The percentage of cell viability was calculated in relation to the control, which was considered as 100% viability. Data represented are means  $\pm$  SD of three independent experiments. Data were analyzed by one-way ANOVA followed by post-hoc comparisons (Tukey).



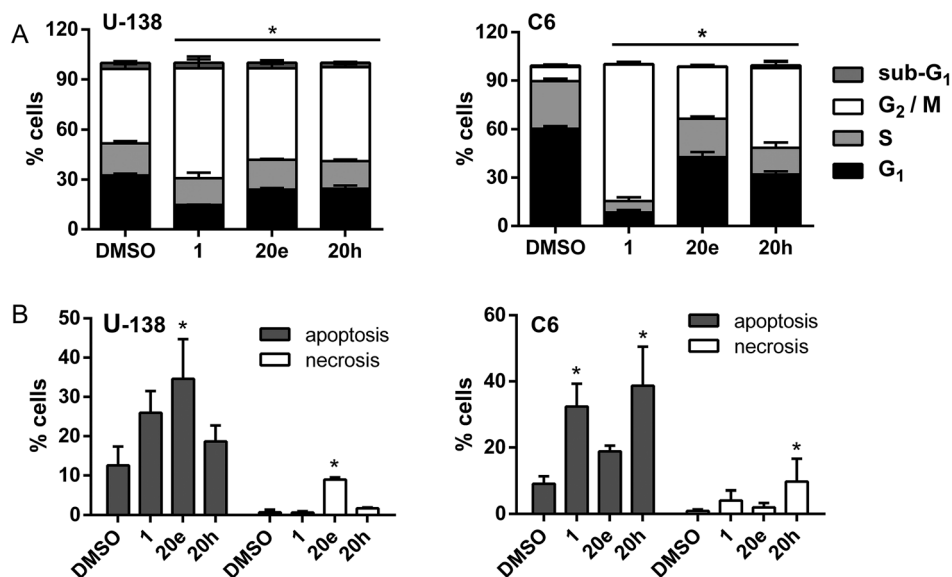


**Fig. 7** (A) Cell-cycle analysis: the cells were treated with the IC<sub>50</sub> concentrations of the molecules; U138 cells were treated with 200  $\mu$ M monastrol 1 or 150  $\mu$ M of 20e or 20h. The C6 cells were treated with 100  $\mu$ M monastrol 1 or 50  $\mu$ M of 20e or 20h for 24 h. After treatment, the cells were permeabilized and stained with propidium iodide for determination of cell-cycle distribution (sub-G<sub>1</sub>, G<sub>0</sub>/G<sub>1</sub>, S and G<sub>2</sub>/M) by flow cytometry. (B) Cell death: the cells were treated with the same concentrations cited above for 48 hours. Cell death was measured by flow cytometry with annexin V/propidium iodide staining. Data were analyzed by FLOWJO® software. Data are representative of cells in necrosis or total apoptosis (early plus late apoptosis). The values presented are the mean  $\pm$  SD and were analyzed by one-way ANOVA followed by post-hoc comparisons (Tukey).

**In vivo toxicological investigation.** A representation of the concentration–response curves for each molecule is depicted in Fig. 9. The results showed that monastrol 1 with LC<sub>50</sub> = 80.11 mM is the safest compound; however, the other compounds also presented safe profiles (20e, LC<sub>50</sub> = 32.90 mM

and 20h, LC<sub>50</sub> = 29.80 mM). This is an important finding because it is the first time that the *in vivo* toxicity of monastrol and DHPMs in *C. elegans* has been revealed. Overall, the molecules presented high LC<sub>50</sub> values, reiterating their safety for use as potential drugs for an *in vivo* glioma model.

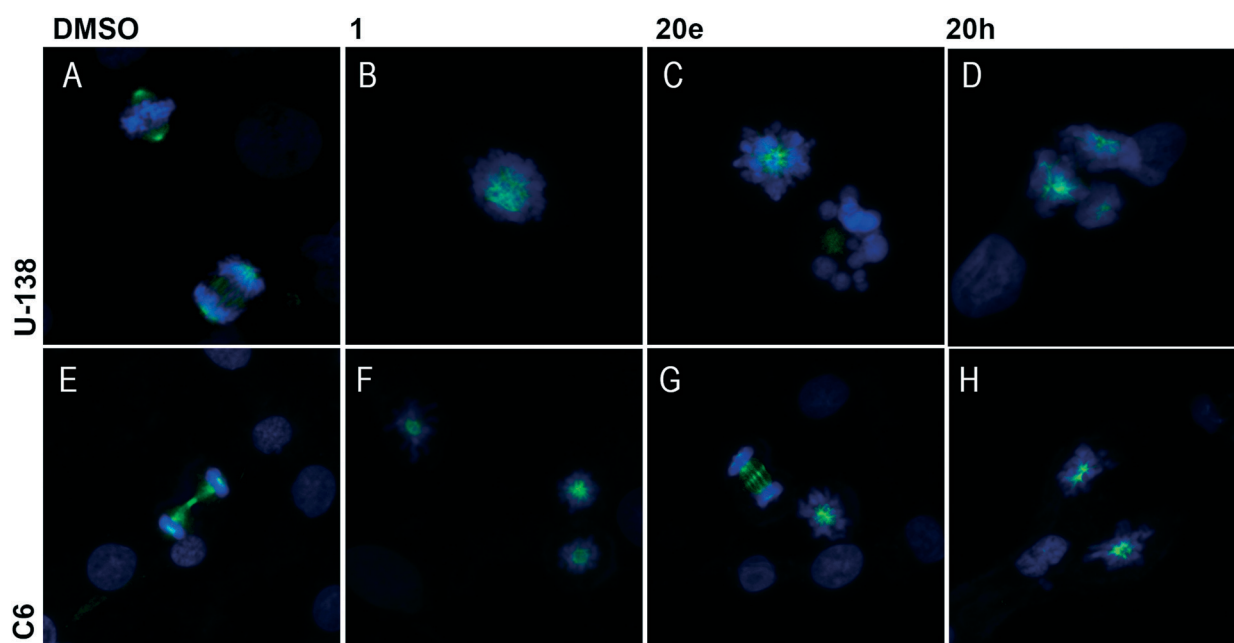


**Fig. 8** Immunocytochemistry: U138 cells (A–D) were treated with 200  $\mu$ M monastrol 1 or 150  $\mu$ M of 20e or 20h, while C6 cells (E–H) were treated with 100  $\mu$ M monastrol 1 or 50  $\mu$ M of 20e or 20h for 24 hours. Fixed cells were stained for DNA (blue) and  $\alpha$ -tubulin (green). The images correspond to a magnification of 600 $\times$ . Imaging was performed on an Olympus FluoView™ 1000 197 confocal microscope.

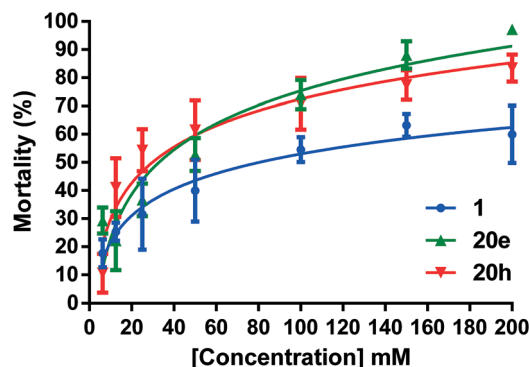


Fig. 9 Mortality percentages of monastrol and its derivatives. Data are presented as mean  $\pm$  SD,  $N = 3$ .

The  $LC_{50}$  values of these compounds are relatively high in comparison to those of other organic molecules tested in worms.<sup>43,44</sup> The low toxicity of monastrol and its derivatives is relevant for future studies of their biological effects in worm models of hyperplasia, which will be further pursued by the present group.

## Conclusions

A novel library of 22 N-1 aryl dihydropyrimidin-2-thiones (19a–k, 20a–k) was synthesized using a forward synthetic route with the aim of generating monastrol derivatives with anticancer activity against glioma cell lines. The molecular modeling studies were conducted with modifications at the N-1 position in order to increase interactions with the P3 pocket, resulting in excellent Eg5 inhibition. The binding poses predicted by GOLD appear to be in accordance with the inhibition studies. It has been demonstrated here that the two new N-1 aryl substituted compounds, 20h and 20e, have about twice the amount of activity of monastrol 1 against glioma cells, confirming the success of N-1 aromatic ring insertion in DHPMs. The greater enzyme inhibition may lead to cell cycle arrest and apoptosis induction without toxicological effects. All these findings present two new dihydropyrimidin-2-thiones, 20h and 20e, as Eg5 kinesin inhibitors and new anti-glioma drug candidates with higher potential than monastrol. Further molecular studies have been developed in order to predict the binding affinities of these ligands in Eg5 as well as *in vivo* analysis using a rat glioma model.

## Experimental

### Chemical analysis

All chemicals were research grade and were used as obtained. Nuclear magnetic resonance spectra ( $^1\text{H}$  NMR and  $^{13}\text{C}$  NMR) were recorded on an Anasazi spectrometer with standard pulse sequences operating at 60 MHz for  $^1\text{H}$  NMR and 15 MHz for  $^{13}\text{C}$  NMR and on a Bruker Ascend NMR with standard pulse sequences operating at 400 MHz for  $^1\text{H}$  NMR and 100 MHz for  $^{13}\text{C}$  NMR, using  $\text{DMSO}-d_6$  or  $\text{CDCl}_3$  as solvent.

Chemical shifts are reported as  $\delta$  values (ppm) relative to TMS (0.0 ppm). The NMR multiplicities brs, s, d, t, q, and m stand for broad singlet, singlet, doublet, triplet, quartet and multiplet, respectively.

The samples were analyzed by a high-resolution mass spectrometer (HR-MS), LTQ-Orbitrap XL (Thermo Scientific), operating at atmospheric pressure ionization (API) with an electrospray ionization (ESI) source. Positive ions  $[\text{M} + \text{H}]^+$  were obtained by applying 4.5 kV to the ion source, 30 V to the capillary and 120 V to the tube lens. The ions were fragmented by collision-induced dissociation (CID) with a normalized collision energy of 20. Nitrogen was used to desolvate the samples at flow rates of 30 and 5 arbitrary units in the sheath and auxiliary gas, respectively. The samples were dissolved in methanol (HPLC-grade, J.T. Baker) at  $50 \mu\text{g mL}^{-1}$  and placed in chromatographic vials. The infusion was aided by ultra-high performance liquid chromatography (UHPLC – Acquity-Waters) at  $100 \mu\text{L min}^{-1}$  using methanol–water (60:40, v/v) without any chromatographic column. The mass resolution was set at 15 000 FWHM (full width at half maximum) and, for accuracy, the HR-MS was externally calibrated ( $m/z$  100 to 2000) just before the analysis with a Pierce™ LTQ ESI Positive Ion (caffeine, MRFA, Ultramark-1621) calibration solution (Thermo-Fisher).

FT-IR spectra were recorded on a Perkin Elmer BXII spectrometer using an ATR probe. TLC analyses were performed on Merck silica plates (60 F254). Melting points (mp) were determined on a System Kofler type WME apparatus and are uncorrected. The term “room temperature” indicates  $20^\circ\text{C}$  to  $30^\circ\text{C}$ . All products were identified through their spectroscopic data and their melting points.

### General preparation of substituted arylthioureas (16a–k)

To a solution of ammonium thiocyanate (1.1 equiv.) in dry acetone at room temperature, benzoyl chloride (1 equiv.) was added, and the solution was heated at  $70^\circ\text{C}$  for 15 minutes. Then, different anilines (1 equiv.) in acetone were added dropwise, and the solution was heated for a further 30 minutes. The reaction mixture was poured into water at room temperature and the precipitate was filtered and submitted to alkaline hydrolysis in NaOH 2.50 M,  $90^\circ\text{C}$  for 20 minutes. Following this, the pH of the system was adjusted to 2 with HCl and 8 with  $\text{NH}_4\text{OH}$ . The product was filtered to a high level of purity.

### General preparation of N-1 aryl substituted dihydropyrimidin-2-thiones

A mixture of ethyl acetoacetate (1 equiv.), substituted phenylthiourea (1 equiv.) and benzaldehyde or 3-hydroxybenzaldehyde (1 equiv.) was solubilized in DMF under ultrasound for 1 hour. TMSCl (6 equiv.) was then added dropwise, and the mixture was stirred at room temperature for 72 h. After three volumes of water were poured into the mixture, it was submitted to ultrasound for one hour; the obtained precipitate was filtered and washed with water. The crude isolate

was recrystallized from ethanol or purified by column chromatography.

**Ethyl 6-methyl-1,4-diphenyl-2-thioxo-1,2,3,4-tetrahydropyrimidine-5-carboxylate (19a).** Green solid, yield 97%, mp: 106 °C to 108 °C. FT-IR (ATR  $\text{cm}^{-1}$ ): 3160 (NH); 1683 (C=O); 1646 (C=C); 1174 (C-O). RMN  $^1\text{H}$  ( $\text{CDCl}_3$ , 60 MHz,  $\delta$  ppm): 1.18 (t,  $^3J = 7.0$  Hz, 3H,  $\text{CH}_3$ ); 2.10 (s, 3H,  $\text{CH}_3$ ); 4.14 (q,  $^3J = 7.0$  Hz, 2H,  $\text{CH}_2$ ); 5.46 (m, 1H, CH); 6.94–7.62 (m,  $10\text{H}_{\text{arom}}$ ); 8.43 (bs, 1H, NH). RMN  $^{13}\text{C}$  ( $\text{CDCl}_3$ , 15 MHz,  $\delta$  ppm): 13.9 ( $\text{CH}_3$ ); 18.4 ( $\text{CH}_3$ ); 53.8 (CH); 60.5 ( $\text{CH}_2$ ); 106.7 (C); 126.3 (C-arom); 127.9 (C-arom); 128.6 (C-arom); 128.8 (C-arom); 140.2 (C-arom); 142.0 (C-arom); 146.2 (C); 165.6 (C); 178.0 (C). HRMS/MS ( $m/z$ ): calcd.  $\text{C}_{20}\text{H}_{20}\text{N}_2\text{O}_2\text{S}$  [ $\text{M} + \text{H}$ ] $^+$ : 353.13182, found 353.13185.

**Ethyl 4-(3-hydroxyphenyl)-6-methyl-1-phenyl-2-thioxo-1,2,3,4-tetrahydropyrimidine-5-carboxylate (20a).** Yellow solid, yield 69%, mp: 151 °C to 154 °C. FT-IR (ATR  $\text{cm}^{-1}$ ): 3278 (OH); 1681 (C=O); 1629 (C=C); 1167 (C-O). RMN  $^1\text{H}$  ( $\text{CDCl}_3$ , 60 MHz,  $\delta$  ppm): 1.19 (t,  $^3J = 7.0$  Hz, 3H,  $\text{CH}_3$ ); 2.08 (s, 3H,  $\text{CH}_3$ ); 4.14 (q,  $^3J = 7.0$  Hz, 2H,  $\text{CH}_2$ ); 5.40 (m, 1H, CH); 6.59–7.56 (m,  $9\text{H}_{\text{arom}}$ ); 7.96 (bs, 1H, NH). RMN  $^{13}\text{C}$  ( $\text{CDCl}_3$ , 15 MHz,  $\delta$  ppm): 14.0 ( $\text{CH}_3$ ); 18.6 ( $\text{CH}_3$ ); 54.1 (CH); 60.9 ( $\text{CH}_2$ ); 106.9 (C); 113.5 (C-arom); 115.4 (C-arom); 118.2 (C-arom); 128.8 (C-arom); 129.1 (C-arom); 130.0 (C-arom); 140.0 (C-arom); 143.6 (C-arom); 146.2 (C); 156.5 (C-arom); 166.1 (C); 178.1 (C). HRMS/MS ( $m/z$ ): calcd.  $\text{C}_{20}\text{H}_{20}\text{N}_2\text{O}_3\text{S}$  [ $\text{M} + \text{H}$ ] $^+$ : 369.12674, found 369.12673.

**Ethyl 1-(4-chlorophenyl)-6-methyl-4-phenyl-2-thioxo-1,2,3,4-tetrahydropyrimidine-5-carboxylate (19b).** Yellow solid, yield 59%, mp: 133 °C to 136 °C. FT-IR (ATR  $\text{cm}^{-1}$ ): 3172 (NH); 1705 (C=O); 1630 (C=C); 1167 (C-O). RMN  $^1\text{H}$  ( $\text{CDCl}_3$ , 60 MHz,  $\delta$  ppm): 1.17 (t,  $^3J = 7.0$  Hz, 3H,  $\text{CH}_3$ ); 2.08 (s, 3H,  $\text{CH}_3$ ); 4.11 (q,  $^3J = 7.0$  Hz, 2H,  $\text{CH}_2$ ); 5.44 (d,  $^3J = 3.0$  Hz, 1H, CH); 6.92–7.51 (m,  $9\text{H}_{\text{arom}}$ ); 8.63 (d,  $^3J = 3.0$  Hz, 1H, NH). RMN  $^{13}\text{C}$  ( $\text{CDCl}_3$ , 15 MHz,  $\delta$  ppm): 14.1 ( $\text{CH}_3$ ); 18.6 ( $\text{CH}_3$ ); 54.2 (CH); 60.8 ( $\text{CH}_2$ ); 107.3 (C); 126.4 (C-arom); 128.2 (C-arom); 128.9 (C-arom); 129.3 (C-arom); 131.4 (C-arom); 138.9 (C-arom); 142.0 (C-arom); 145.7 (C); 165.6 (C); 178.2 (C). HRMS/MS ( $m/z$ ): calcd.  $\text{C}_{20}\text{H}_{19}\text{ClN}_2\text{O}_2\text{S}$  [ $\text{M} + \text{H}$ ] $^+$ : 387.09285, found 387.09260.

**Ethyl 1-(4-chlorophenyl)-4-(3-hydroxyphenyl)-6-methyl-2-thioxo-1,2,3,4-tetrahydropyrimidine-5-carboxylate (20b).** White solid, yield 25%, mp: 163 °C to 167 °C. FT-IR (ATR  $\text{cm}^{-1}$ ): 3379 (OH); 3165 (NH); 1691 (C=O); 1639 (C=C); 1174 (C-O). RMN  $^1\text{H}$  ( $\text{CDCl}_3$ , 60 MHz,  $\delta$  ppm): 1.18 (t,  $^3J = 7.0$  Hz, 3H,  $\text{CH}_3$ ); 2.06 (s, 3H,  $\text{CH}_3$ ); 4.04 (q,  $^3J = 7.0$  Hz, 2H,  $\text{CH}_2$ ); 5.38 (d,  $^3J = 3.0$  Hz, 1H, CH); 6.20–7.45 (m,  $8\text{H}_{\text{arom}}$ ); 7.964 (d,  $^3J = 3.0$  Hz, 1H, NH). RMN  $^{13}\text{C}$  ( $\text{DMSO}-d_6$ , 15 MHz,  $\delta$  ppm): 14.0 ( $\text{CH}_3$ ); 18.2 ( $\text{CH}_3$ ); 53.3 (CH); 60.3 ( $\text{CH}_2$ ); 105.9 (C); 113.2 (C-arom); 115.0 (C-arom); 117.0 (C-arom); 128.8 (C-arom); 129.8 (C-arom); 132.3 (C-arom); 133.0 (C-arom); 139.3 (C-arom); 144.1; 145.6; 157.9 (C-arom); 165.3 (C); 177.1 (C). HRMS/MS ( $m/z$ ): calcd.  $\text{C}_{20}\text{H}_{19}\text{ClN}_2\text{O}_3\text{S}$  [ $\text{M} + \text{H}$ ] $^+$ : 403.08776, found 403.08705.

**Ethyl 1-(3-chlorophenyl)-6-methyl-4-phenyl-2-thioxo-1,2,3,4-tetrahydropyrimidine-5-carboxylate (19c).** White solid,

yield 34%, mp: 130 °C to 135 °C. FT-IR (ATR  $\text{cm}^{-1}$ ): 3176 (NH); 1701 (C=O); 1628 (C=C); 1171 (C-O). RMN  $^1\text{H}$  ( $\text{CDCl}_3$ , 60 MHz,  $\delta$  ppm): 1.16 (t,  $^3J = 7.0$  Hz, 3H,  $\text{CH}_3$ ); 2.09 (s, 3H,  $\text{CH}_3$ ); 4.12 (q,  $^3J = 7.0$  Hz, 2H,  $\text{CH}_2$ ); 5.45 (d,  $^3J = 3.0$  Hz, 1H, CH); 6.97–7.51 (m,  $9\text{H}_{\text{arom}}$ ); 8.75 (d,  $^3J = 3.0$  Hz, 1H, NH). RMN  $^{13}\text{C}$  ( $\text{CDCl}_3$ , 15 MHz,  $\delta$  ppm): 14.1 ( $\text{CH}_3$ ); 18.6 ( $\text{CH}_3$ ); 54.1 (CH); 60.7 ( $\text{CH}_2$ ); 107.2 (C); 126.4 (C-arom); 128.1 (C-arom); 128.9 (C-arom); 129.0 (C-arom); 129.8 (C-arom); 134.4 (C-arom); 141.4 (C-arom); 142.0 (C-arom); 145.5 (C); 165.6 (C); 177.9 (C). HRMS/MS ( $m/z$ ): calcd.  $\text{C}_{20}\text{H}_{19}\text{ClN}_2\text{O}_2\text{S}$  [ $\text{M} + \text{H}$ ] $^+$ : 387.09285, found 387.09296.

**Ethyl 1-(3-chlorophenyl)-4-(3-hydroxyphenyl)-6-methyl-2-thioxo-1,2,3,4-tetrahydropyrimidine-5-carboxylate (20c).** Yellow solid, yield 40%, mp: 75 °C to 80 °C. FT-IR (ATR  $\text{cm}^{-1}$ ): 3280 (OH); 1684 (C=O); 1631 (C=C); 1169 (C-O). RMN  $^1\text{H}$  ( $\text{CDCl}_3$ , 60 MHz,  $\delta$  ppm): 1.19 (t,  $^3J = 7.0$  Hz, 3H,  $\text{CH}_3$ ); 2.08 (s, 3H,  $\text{CH}_3$ ); 4.14 (q,  $^3J = 7.0$  Hz, 2H,  $\text{CH}_2$ ); 5.40 (d,  $^3J = 3.0$  Hz, 1H, CH); 6.58–7.48 (m,  $8\text{H}_{\text{arom}}$ ); 7.84 (d,  $^3J = 3.0$  Hz, 1H, NH). RMN  $^{13}\text{C}$  ( $\text{CDCl}_3$ , 15 MHz,  $\delta$  ppm): 14.0 ( $\text{CH}_3$ ); 18.7 ( $\text{CH}_3$ ); 54.2 (CH); 61.0 ( $\text{CH}_2$ ); 107.2 (C); 113.4 (C-arom); 115.5 (C-arom); 118.2 (C-arom); 129.2 (C-arom); 130.1 (C-arom); 134.5 (C-arom); 141.2 (C-arom); 143.4 (C-arom); 145.0 (C); 156.5 (C-arom); 165.9 (C); 177.8 (C). HRMS/MS ( $m/z$ ): calcd.  $\text{C}_{20}\text{H}_{19}\text{ClN}_2\text{O}_3\text{S}$  [ $\text{M} + \text{H}$ ] $^+$ : 403.08776, found 403.08790.

**Ethyl 1-(4-bromophenyl)-6-methyl-4-phenyl-2-thioxo-1,2,3,4-tetrahydropyrimidine-5-carboxylate (19d).** Yellow solid, yield 83%, mp: 117 °C to 122 °C. FT-IR (ATR  $\text{cm}^{-1}$ ): 3169 (NH); 1699 (C=O); 1631 (C=C); 1166 (C-O). RMN  $^1\text{H}$  ( $\text{CDCl}_3$ , 60 MHz,  $\delta$  ppm): 1.19 (t,  $^3J = 7.0$  Hz, 3H,  $\text{CH}_3$ ); 2.09 (s, 3H,  $\text{CH}_3$ ); 4.14 (q,  $^3J = 7.0$  Hz, 2H,  $\text{CH}_2$ ); 5.46 (d,  $^3J = 3.0$  Hz, 1H, CH); 6.95–7.66 (m,  $9\text{H}_{\text{arom}}$ ); 8.03 (d,  $^3J = 3.0$  Hz, 1H, NH). RMN  $^{13}\text{C}$  ( $\text{CDCl}_3$ , 15 MHz,  $\delta$  ppm): 13.9 ( $\text{CH}_3$ ); 18.4 ( $\text{CH}_3$ ); 53.9 (CH); 60.5 ( $\text{CH}_2$ ); 107.1 (C); 122.6 (C-arom); 126.2 (C-arom); 127.9 (C-arom); 128.7 (C-arom); 131.6 (C-arom); 132.1 (C-arom); 139.2 (C-arom); 141.8 (C-arom); 145.4 (C); 165.4 (C); 177.8 (C). HRMS/MS ( $m/z$ ): calcd.  $\text{C}_{20}\text{H}_{19}\text{BrN}_2\text{O}_2\text{S}$  [ $\text{M} + \text{H}$ ] $^+$ : 431.04232, found 431.04236.

**Ethyl 1-(4-bromophenyl)-4-(3-hydroxyphenyl)-6-methyl-2-thioxo-1,2,3,4-tetrahydropyrimidine-5-carboxylate (20d).** White solid, yield 98%, mp: 144 °C to 149 °C. FT-IR (ATR  $\text{cm}^{-1}$ ): 3380 (OH); 3175 (NH); 1692 (C=O); 1641 (C=C); 1169 (C-O). RMN  $^1\text{H}$  ( $\text{CDCl}_3$ , 60 MHz,  $\delta$  ppm): 1.18 (t,  $^3J = 7.0$  Hz, 3H,  $\text{CH}_3$ ); 2.08 (s, 3H,  $\text{CH}_3$ ); 4.14 (q,  $^3J = 7.0$  Hz, 2H,  $\text{CH}_2$ ); 5.37 (m, 1H, CH); 6.71–7.06 (m,  $4\text{H}_{\text{arom}}$ ); 7.06–7.35 (m,  $2\text{H}_{\text{arom}}$ ); 7.35–7.72 (m,  $2\text{H}_{\text{arom}}$ ); 8.14 (bs, 1H, NH). RMN  $^{13}\text{C}$  ( $\text{CDCl}_3$ , 15 MHz,  $\delta$  ppm): 13.9 ( $\text{CH}_3$ ); 18.7 ( $\text{CH}_3$ ); 53.6 (CH); 60.7 ( $\text{CH}_2$ ); 106.2 (C); 112.2 (C-arom); 114.4 (C-arom); 117.1 (C-arom); 121.6 (C-arom); 128.8 (C-arom); 130.5 (C-arom); 131.0 (C-arom); 137.8 (C-arom); 141.9 (C-arom); 144.1 (C); 154.8 (C-arom); 164.2 (C); 176.0 (C). HRMS/MS ( $m/z$ ): calcd.  $\text{C}_{20}\text{H}_{19}\text{BrN}_2\text{O}_3\text{S}$  [ $\text{M} + \text{H}$ ] $^+$ : 447.03724, found 447.03760.

**Ethyl 6-methyl-1-(4-nitrophenyl)-4-phenyl-2-thioxo-1,2,3,4-tetrahydropyrimidine-5-carboxylate (19e).** Yellow solid, yield 50%, mp: 208 °C to 211 °C. FT-IR (ATR  $\text{cm}^{-1}$ ): 3162 (NH); 1702 (C=O); 1649 (C=C); 1518 (N=O); 1346 (N=O); 1181 (C-O). RMN  $^1\text{H}$  ( $\text{DMSO}-d_6$ , 60 MHz,  $\delta$  ppm): 1.13 (t,  $^3J = 7.0$



Hz, 3H, CH<sub>3</sub>); 2.06 (s, 3H, CH<sub>3</sub>); 4.15 (q, <sup>3</sup>J = 7.0 Hz, 2H, CH<sub>2</sub>); 5.35 (d, <sup>3</sup>J = 4.0 Hz, 1H, CH); 7.32–7.78; (m, 7H<sub>arom</sub>); 8.16–8.47 (m, 2H<sub>arom</sub>); 10.19 (d, <sup>3</sup>J = 3.0 Hz, 1H, NH). RMN C<sup>13</sup> (DMSO-d<sub>6</sub>, 15 MHz, δ ppm): 13.9 (CH<sub>3</sub>); 18.2 (CH<sub>3</sub>); 53.5 (CH); 60.3 (CH<sub>2</sub>); 105.9 (C); 123.3 (C-arom); 126.5 (C-arom); 127.9 (C-arom); 128.8 (C-arom); 132.1 (C-arom); 142.5 (C-arom); 145.1 (C-arom); 146.9 (C); 146.9 (C-arom); 165.1 (C); 176.5 (C). HRMS/MS (*m/z*): calcd. C<sub>20</sub>H<sub>19</sub>N<sub>3</sub>O<sub>4</sub>S [M + H]<sup>+</sup>: 398.11690, found 398.11704.

**Ethyl 4-(3-hydroxyphenyl)-6-methyl-1-(4-nitrophenyl)-2-thioxo-1,2,3,4-tetrahydropyrimidine-5-carboxylate (20e).** Yellow solid, yield 70%, mp: 200 °C to 202 °C. FT-IR (ATR cm<sup>-1</sup>): 3147 (NH); 1707 (C=O); 1641 (C=C); 1518 (N=O); 1344 (N=O); 1173 (C-O). RMN H<sup>1</sup> (DMSO-d<sub>6</sub>, 60 MHz, δ ppm): 1.14 (t, <sup>3</sup>J = 7.0 Hz, 3H, CH<sub>3</sub>); 2.03 (s, 3H, CH<sub>3</sub>); 4.09 (q, <sup>3</sup>J = 7.0 Hz, 2H, CH<sub>2</sub>); 5.24 (d, <sup>3</sup>J = 3.0 Hz, 1H, CH); 6.58–7.72 (m, 6H<sub>arom</sub>); 8.14–8.51 (m, 2H<sub>arom</sub>); 9.54 (s, 1H, OH); 10.12 (d, <sup>3</sup>J = 3.0 Hz, 1H, NH). RMN C<sup>13</sup> (DMSO-d<sub>6</sub>, 15 MHz, δ ppm): 13.9 (CH<sub>3</sub>); 18.2 (CH<sub>3</sub>); 53.4 (CH); 60.3 (CH<sub>2</sub>); 106.2 (C); 113.3 (C-arom); 115.0 (C-arom); 117.0 (C-arom); 123.9 (C-arom); 129.8 (C-arom); 132.2 (C-arom); 143.9 (C-arom); 144.9 (C-arom); 146.2; 147.0; 157.8 (C-arom); 165.2 (C); 176.4 (C). HRMS/MS (*m/z*): calcd. C<sub>20</sub>H<sub>19</sub>N<sub>3</sub>O<sub>5</sub>S [M + H]<sup>+</sup>: 414.11181, found 414.11198.

**Ethyl 6-methyl-4-phenyl-2-thioxo-1-(3-(trifluoromethyl)phenyl)-1,2,3,4-tetrahydropyrimidine-5-carboxylate (19f).** Green solid, yield 42%, mp: 103 °C to 109 °C. FT-IR (ATR cm<sup>-1</sup>): 3166 (NH); 1700 (C=O); 1649 (C=C); 1163 (C-O). RMN H<sup>1</sup> (CDCl<sub>3</sub>, 400 MHz, δ ppm): 1.22 (t, <sup>3</sup>J = 7.1 Hz, 3H, CH<sub>3</sub>); 2.11 (s, 3H, CH<sub>3</sub>); 4.17 (m, 2H, CH<sub>2</sub>); 5.52 (d, <sup>3</sup>J = 3.6 Hz, 1H, CH); 7.45–7.32 (m, 6H<sub>arom</sub>); 7.75–7.56 (m, 3H); 8.01 (d, <sup>3</sup>J = 3.0 Hz, 2H). RMN C<sup>13</sup> (CDCl<sub>3</sub>, 100 MHz, δ ppm): 14.1 (CH<sub>3</sub>); 18.2 (CH<sub>3</sub>); 54.6 (CH); 60.9 (CH<sub>2</sub>); 107.7 (C); 122.1; 124.8; 125.7; 126.4; 128.4; 129.1; 141.0; 141.9; 145.2; 165.5; 178.4. HRMS/MS (*m/z*): calcd. C<sub>21</sub>H<sub>19</sub>F<sub>3</sub>N<sub>2</sub>O<sub>2</sub>S [M + H]<sup>+</sup>: 421.11920, found 421.11918.

**Ethyl 4-(3-hydroxyphenyl)-6-methyl-2-thioxo-1-(3-(trifluoromethyl)phenyl)-1,2,3,4-tetrahydropyrimidine-5-carboxylate (20f).** Yellow solid, yield 27%, mp: 70 °C to 74 °C. FT-IR (ATR cm<sup>-1</sup>): 3291 (NH); 1683 (C=O); 1634 (C=C); 1165 (C-O). RMN H<sup>1</sup> (CDCl<sub>3</sub>, 400 MHz, δ ppm): 1.19 (t, <sup>3</sup>J = 7.1 Hz, 3H, CH<sub>3</sub>); 2.05 (s, 3H, CH<sub>3</sub>); 4.14 (q, <sup>3</sup>J = 7.0 Hz, 2H, CH<sub>2</sub>); 5.41 (d, <sup>3</sup>J = 3.3 Hz, 1H, CH); 6.74 (m, 1H<sub>arom</sub>); 6.85 (m, 1H<sub>arom</sub>); 7.15 (t, <sup>3</sup>J = 7.8 Hz, 1H); 7.53 (m, 2H<sub>arom</sub>); 7.66 (m, 1H<sub>arom</sub>); 8.09 (d, <sup>3</sup>J = 3.2 Hz, 1H, NH). RMN C<sup>13</sup> (CDCl<sub>3</sub>, 100 MHz, δ ppm): 14.2 (CH<sub>3</sub>); 19.0 (CH<sub>3</sub>); 54.5 (CH); 61.3 (CH<sub>2</sub>); 107.8 (C); 113.6; 115.8; 118.5; 122.3; 125.0; 125.9; 130.4; 141.0; 143.5; 145.3; 156.5; 165.9; 178.3. HRMS/MS (*m/z*): calcd. for C<sub>21</sub>H<sub>19</sub>F<sub>3</sub>N<sub>2</sub>O<sub>3</sub>S [M + H]<sup>+</sup>: 437.11412, found 437.11395.

**Ethyl 1-(4-hydroxyphenyl)-6-methyl-4-phenyl-2-thioxo-1,2,3,4-tetrahydropyrimidine-5-carboxylate (19g).** Brown solid, yield 52%, mp: 173 °C to 177 °C. FT-IR (ATR cm<sup>-1</sup>): 3212 (OH); 1697 (C=O); 1649 (C=C); 1173 (C-O). RMN H<sup>1</sup> (DMSO-d<sub>6</sub>, 60 MHz, δ ppm): 1.14 (t, <sup>3</sup>J = 7.0 Hz, 3H, CH<sub>3</sub>); 2.08 (s, 3H, CH<sub>3</sub>); 4.07 (q, <sup>3</sup>J = 7.0 Hz, 2H, CH<sub>2</sub>); 5.27 (d, <sup>3</sup>J =

3.0 Hz, 1H, CH); 6.48–7.09 (m, 4H<sub>arom</sub>); 7.10–7.48 (m, 5H<sub>arom</sub>); 9.67 (s, 1H, OH); 9.92 (d, <sup>3</sup>J = 3.0 Hz, 1H, NH). RMN C<sup>13</sup> (DMSO-d<sub>6</sub>, 15 MHz, δ ppm): 13.7 (CH<sub>3</sub>); 18.2 (CH<sub>3</sub>); 52.9 (CH); 60.1 (CH<sub>2</sub>); 105.5 (C); 115.2 (C-arom); 126.3 (C-arom); 127.8 (C-arom); 128.8 (C-arom); 131.6 (C-arom); 142.9 (C-arom); 147.0 (C); 157.1 (C-arom); 165.3 (C); 177.8 (C). HRMS/MS (*m/z*): calcd. C<sub>20</sub>H<sub>20</sub>N<sub>2</sub>O<sub>3</sub>S [M + H]<sup>+</sup>: 369.12673, found 369.12665.

**Ethyl 4-(3-hydroxyphenyl)-1-(4-hydroxyphenyl)-6-methyl-2-thioxo-1,2,3,4-tetrahydropyrimidine-5-carboxylate (20g).** Yellow solid, yield 48%, mp: 198 °C to 201 °C. FT-IR (ATR cm<sup>-1</sup>): 3150 (OH); 1697 (C=O); 1650 (C=C); 1183 (C-O). RMN H<sup>1</sup> (DMSO-d<sub>6</sub>, 60 MHz, δ ppm): 1.13 (t, <sup>3</sup>J = 7.0 Hz, 3H, CH<sub>3</sub>); 2.02 (s, 3H, CH<sub>3</sub>); 4.07 (q, <sup>3</sup>J = 7.0 Hz, 2H, CH<sub>2</sub>); 5.17 (d, <sup>3</sup>J = 3.0 Hz, 1H, CH); 6.52–7.35 (m, 8H<sub>arom</sub>); 9.49 (s, 1H, OH); 9.65 (s, 1H, OH); 9.84 (d, <sup>3</sup>J = 3.0 Hz, 1H, NH). RMN C<sup>13</sup> (DMSO-d<sub>6</sub>, 15 MHz, δ ppm): 14.0 (CH<sub>3</sub>); 18.2 (CH<sub>3</sub>); 53.5 (CH); 60.2 (CH<sub>2</sub>); 105.6 (C); 113.2 (C-arom); 115.2 (C-arom); 117.0 (C-arom); 129.7 (C-arom); 131.9 (C-arom); 144.5 (C-arom); 146.7 (C); 157.2 (C-arom); 157.7 (C-arom); 165.6 (C); 177.8 (C). HRMS/MS (*m/z*): calcd. C<sub>20</sub>H<sub>20</sub>N<sub>2</sub>O<sub>4</sub>S [M + H]<sup>+</sup>: 385.12165, found 385.12155.

**Ethyl 1-(4-methoxyphenyl)-6-methyl-4-phenyl-2-thioxo-1,2,3,4-tetrahydropyrimidine-5-carboxylate (19h).** Green solid, yield 77%, mp: 144 °C to 148 °C. FT-IR (ATR cm<sup>-1</sup>): 3170 (NH); 1703 (C=O); 1630 (C=C); 1157 (C-O). RMN H<sup>1</sup> (CDCl<sub>3</sub>, 60 MHz, δ ppm): 1.19 (t, <sup>3</sup>J = 7.0 Hz, 3H, CH<sub>3</sub>); 2.11 (s, 3H, CH<sub>3</sub>); 3.83 (s, 3H, CH<sub>3</sub>); 4.14 (q, <sup>3</sup>J = 7.0 Hz, 2H, CH<sub>2</sub>); 5.46 (d, <sup>3</sup>J = 3.0 Hz, 1H, CH); 6.79–7.40 (m, 9H<sub>arom</sub>); 7.87 (d, <sup>3</sup>J = 3.0 Hz, 1H, NH). RMN C<sup>13</sup> (CDCl<sub>3</sub>, 15 MHz, δ ppm): 14.1 (CH<sub>3</sub>); 18.5 (CH<sub>3</sub>); 53.9 (CH); 55.4 (CH<sub>3</sub>); 60.6 (CH<sub>2</sub>); 106.8 (C); 114.1 (C-arom); 126.4 (C-arom); 128.0 (C-arom); 128.8 (C-arom); 133.2 (C-arom); 142.3 (C-arom); 146.7 (C); 159.4 (C-arom); 165.7 (C); 178.7 (C). HRMS/MS (*m/z*): calcd. C<sub>21</sub>H<sub>22</sub>N<sub>2</sub>O<sub>3</sub>S [M + H]<sup>+</sup>: 383.14238, found 383.14242.

**Ethyl 4-(3-hydroxyphenyl)-1-(4-methoxyphenyl)-6-methyl-2-thioxo-1,2,3,4-tetrahydropyrimidine-5-carboxylate (20h).** Green solid, yield 60%, mp: 174 °C to 177 °C. FT-IR (ATR cm<sup>-1</sup>): 3147 (NH); 1652 (C=O); 1622 (C=C); 1171 (C-O). RMN H<sup>1</sup> (DMSO-d<sub>6</sub>, 60 MHz, δ ppm): 1.16 (t, <sup>3</sup>J = 7.0 Hz, 3H, CH<sub>3</sub>); 2.04 (s, 3H, CH<sub>3</sub>); 3.79 (s, 3H, CH<sub>3</sub>); 4.10 (q, <sup>3</sup>J = 7.0 Hz, 2H, CH<sub>2</sub>); 5.31 (d, <sup>3</sup>J = 4.0 Hz, 1H, CH); 6.56–7.35 (m, 8H<sub>arom</sub>); 9.52 (s, 1H, OH); 9.81 (d, <sup>3</sup>J = 4.0 Hz, 1H, NH). RMN C<sup>13</sup> (DMSO-d<sub>6</sub>, 15 MHz, δ ppm): 14.0 (CH<sub>3</sub>); 18.2 (CH<sub>3</sub>); 53.1 (CH); 55.3 (CH<sub>3</sub>); 60.1 (CH<sub>2</sub>); 105.6 (C); 113.2 (C-arom); 113.8 (C-arom); 114.9 (C-arom); 116.9 (C-arom); 129.7 (C-arom); 133.1 (C-arom); 144.2 (C-arom); 146.5 (C); 157.7 (C-arom); 158.7 (C-arom); 165.4 (C); 177.7 (C). HRMS/MS (*m/z*): calcd. C<sub>21</sub>H<sub>22</sub>N<sub>2</sub>O<sub>4</sub>S [M + H]<sup>+</sup>: 399.13730, found 399.13752.

**Ethyl 1-(2,6-dimethylphenyl)-6-methyl-4-phenyl-2-thioxo-1,2,3,4-tetrahydropyrimidine-5-carboxylate (19i).** Yellow solid, yield 62%, mp: 124 °C to 128 °C. FT-IR (ATR cm<sup>-1</sup>): 3176 (NH); 1712 (C=O); 1652 (C=C); 1176 (C-O). RMN H<sup>1</sup> (CDCl<sub>3</sub>, 60 MHz, δ ppm): 1.12 (t, <sup>3</sup>J = 7.0 Hz, 3H, CH<sub>3</sub>); 2.03 (s, 3H, CH<sub>3</sub>); 2.16 (s, 3H, CH<sub>3</sub>); 2.24 (s, 3H, CH<sub>3</sub>); 4.10 (q, <sup>3</sup>J = 7.0 Hz, 2H, CH<sub>2</sub>); 5.52 (m, 1H, CH); 7.06–7.22 (m, 3H<sub>arom</sub>); 7.22–7.49

(m, 5H<sub>arom</sub>); 7.91 (bs, 1H, NH). RMN C<sup>13</sup> (CDCl<sub>3</sub>, 15 MHz,  $\delta$  ppm): 13.6 (CH<sub>3</sub>); 16.6 (CH<sub>3</sub>); 17.6 (CH<sub>3</sub>); 53.9 (CH); 60.0 (CH<sub>2</sub>); 104.9 (C); 126.4 (C-arom); 127.5 (C-arom); 128.2 (C-arom); 135.7 (C-arom); 138.0 (C-arom); 138.3 (C-arom); 142.4 (C-arom); 145.1 (C); 165.4 (C); 175.6 (C). HRMS/MS ( $m/z$ ): calcd. C<sub>22</sub>H<sub>24</sub>N<sub>2</sub>O<sub>2</sub>S [M + H]<sup>+</sup>: 381.16312, found 381.16324.

**Ethyl 1-(2,6-dimethylphenyl)-4-(3-hydroxyphenyl)-6-methyl-2-thioxo-1,2,3,4-tetrahydropyrimidine-5-carboxylate (20i).** Brown solid, yield 69%, mp: 163 °C to 167 °C. FT-IR (ATR cm<sup>-1</sup>): 3166 (OH); 1705 (C=O); 1636 (C=C); 1174 (C-O). RMN H<sup>1</sup> (CDCl<sub>3</sub>, 60 MHz,  $\delta$  ppm): 1.14 (t, <sup>3</sup>J = 7.0 Hz, 3H, CH<sub>3</sub>); 2.00 (s, 3H, CH<sub>3</sub>); 2.12 (s, 3H, CH<sub>3</sub>); 2.24 (s, 3H, CH<sub>3</sub>); 4.11 (q, <sup>3</sup>J = 7.0 Hz, 2H, CH<sub>2</sub>); 5.46 (m, 1H, CH); 6.55–7.31 (m, 7H<sub>arom</sub>); 7.92 (bs, 1H, NH). RMN C<sup>13</sup> (CDCl<sub>3</sub>, 15 MHz,  $\delta$  ppm): 14.0 (CH<sub>3</sub>); 17.1 (CH<sub>3</sub>); 18.1 (CH<sub>3</sub>); 18.2 (CH<sub>3</sub>); 54.6 (CH); 60.8 (CH<sub>2</sub>); 105.6 (C); 114.0 (C-arom); 115.4 (C-arom); 118.4 (C-arom); 128.5 (C-arom); 128.6 (C-arom); 128.9 (C-arom); 130.1 (C-arom); 136.3 (C-arom); 137.3 (C-arom); 138.7 (C-arom); 144.1 (C-arom); 145.3 (C); 156.5 (C-arom); 166.2 (C); 176.3 (C). HRMS/MS ( $m/z$ ): calcd. C<sub>22</sub>H<sub>24</sub>N<sub>2</sub>O<sub>3</sub>S [M + H]<sup>+</sup>: 397.15803, found 397.15898.

**Ethyl 1-(3,5-dimethylphenyl)-6-methyl-4-phenyl-2-thioxo-1,2,3,4-tetrahydropyrimidine-5-carboxylate (19j).** Green solid, yield 64%, mp: 135 °C to 138 °C. FT-IR (ATR cm<sup>-1</sup>): 3167 (NH); 1705 (C=O); 1623 (C=C); 1158 (C-O). RMN H<sup>1</sup> (CDCl<sub>3</sub>, 60 MHz,  $\delta$  ppm): 1.16 (t, <sup>3</sup>J = 7.0 Hz, 3H, CH<sub>3</sub>); 2.10 (s, 3H, CH<sub>3</sub>); 2.32 (s, 6H, 2CH<sub>3</sub>); 4.12 (q, <sup>3</sup>J = 7.0 Hz, 2H, CH<sub>2</sub>); 5.45 (d, <sup>3</sup>J = 3.0 Hz, 1H, CH); 6.45–6.94 (m, 2H<sub>arom</sub>); 7.01 (m, 1H<sub>arom</sub>); 7.15–7.42 (m, 5H<sub>arom</sub>); 8.64 (d, <sup>3</sup>J = 3.0 Hz, 1H, NH). RMN C<sup>13</sup> (CDCl<sub>3</sub>, 15 MHz): 14.1 (CH<sub>3</sub>); 18.6 (CH<sub>3</sub>); 21.2 (2CH<sub>3</sub>); 54.1 (CH); 60.5 (CH<sub>2</sub>); 106.5 (C); 126.5 (C-arom); 128.0 (C-arom); 128.8 (C-arom); 130.4 (C-arom); 138.6 (C-arom); 140.2 (C-arom); 142.4 (C-arom); 146.5 (C); 165.8 (C); 178.2 (C). HRMS/MS ( $m/z$ ): calcd. C<sub>22</sub>H<sub>24</sub>N<sub>2</sub>O<sub>2</sub>S [M + H]<sup>+</sup>: 381.16312, found 381.16310.

**Ethyl 1-(3,5-dimethylphenyl)-4-(3-hydroxyphenyl)-6-methyl-2-thioxo-1,2,3,4-tetrahydropyrimidine-5-carboxylate (20j).** Green solid, yield 55%, mp: 197 °C to 200 °C. FT-IR (ATR cm<sup>-1</sup>): 3168 (OH); 1697 (C=O); 1628 (C=C); 1149 (C-O). RMN H<sup>1</sup> (CDCl<sub>3</sub>, 60 MHz,  $\delta$  ppm): 1.18 (t, <sup>3</sup>J = 7.0 Hz, 3H, CH<sub>3</sub>); 2.08 (s, 3H, CH<sub>3</sub>); 2.31 (s, 6H, 2CH<sub>3</sub>); 4.12 (q, <sup>3</sup>J = 7.0 Hz, 2H, CH<sub>2</sub>); 5.37 (d, <sup>3</sup>J = 3.0 Hz, 1H, CH); 6.40 (m, 1H<sub>arom</sub>); 6.54–7.36 (m, 6H<sub>arom</sub>); 7.89 (d, <sup>3</sup>J = 3.0 Hz, 1H, NH). RMN C<sup>13</sup> (DMSO-d<sub>6</sub>, 15 MHz,  $\delta$  ppm): 14.0 (CH<sub>3</sub>); 18.3 (CH<sub>3</sub>); 20.8 (2CH<sub>3</sub>); 53.2 (CH); 60.2 (CH<sub>2</sub>); 105.6 (C); 113.3 (C-arom); 114.9 (C-arom); 117.1 (C-arom); 129.8 (C-arom); 137.9 (C-arom); 140.2 (C-arom); 144.3 (C-arom); 146.1 (C); 157.7 (C-arom); 165.64 (C); 177.2 (C). HRMS/MS ( $m/z$ ): calcd. C<sub>22</sub>H<sub>24</sub>N<sub>2</sub>O<sub>3</sub>S [M + H]<sup>+</sup>: 397.15803, found 397.15819.

**Ethyl 1-(3,4-dimethylphenyl)-6-methyl-4-phenyl-2-thioxo-1,2,3,4-tetrahydropyrimidine-5-carboxylate (19k).** White solid, yield 55%, mp: 189 °C to 191 °C. FT-IR (ATR cm<sup>-1</sup>): 3181 (NH); 1702 (C=O); 1622 (C=C); 1153 (C-O). RMN H<sup>1</sup> (CDCl<sub>3</sub>, 60 MHz,  $\delta$  ppm): 1.18 (t, <sup>3</sup>J = 7.0 Hz, 3H, CH<sub>3</sub>); 2.10 (s, 3H, CH<sub>3</sub>); 2.28 (s, 6H, 2CH<sub>3</sub>); 4.12 (q, <sup>3</sup>J = 7.0 Hz, 2H, CH<sub>2</sub>); 5.45 (d, <sup>3</sup>J = 3.0 Hz, 1H, CH); 6.71–7.43 (m, 8H<sub>arom</sub>); 8.10 (d, <sup>3</sup>J =

3.0 Hz, 1H, NH). RMN C<sup>13</sup> (CDCl<sub>3</sub>, 15 MHz,  $\delta$  ppm): 13.9 (CH<sub>3</sub>); 18.4 (CH<sub>3</sub>); 19.4 (CH<sub>3</sub>); 19.7 (CH<sub>3</sub>); 53.8 (CH); 60.4 (CH<sub>2</sub>); 106.5 (C); 126.3 (C-arom); 127.8 (C-arom); 128.6 (C-arom); 129.9 (C-arom); 137.1 (C-arom); 137.9 (C-arom); 142.3 (C-arom); 146.5 (C); 165.5 (C); 178.2 (C). HRMS/MS ( $m/z$ ): calcd. C<sub>22</sub>H<sub>24</sub>N<sub>2</sub>O<sub>2</sub>S [M + H]<sup>+</sup>: 381.16312, found 381.16291.

**Ethyl 1-(3,4-dimethylphenyl)-4-(3-hydroxyphenyl)-6-methyl-2-thioxo-1,2,3,4-tetrahydropyrimidine-5-carboxylate (20k).** White solid, yield 57%, mp: 163 °C to 167 °C. FT-IR (ATR cm<sup>-1</sup>): 3364 (OH); 3169 (NH); 1657 (C=O); 1627 (C=C); 1150 (C-O). RMN H<sup>1</sup> (CDCl<sub>3</sub>, 60 MHz,  $\delta$  ppm): 1.17 (t, <sup>3</sup>J = 7.0 Hz, 3H, CH<sub>3</sub>); 2.08 (s, 3H, CH<sub>3</sub>); 2.26 (s, 6H, 2CH<sub>3</sub>); 4.14 (q, <sup>3</sup>J = 7.0 Hz, 2H, CH<sub>2</sub>); 5.38 (d, <sup>3</sup>J = 3.0 Hz, 1H, CH); 6.25–6.54 (m, 1H<sub>arom</sub>); 6.54–7.33 (m, 6H<sub>arom</sub>); 7.92 (d, <sup>3</sup>J = 3.0 Hz, 1H, NH). RMN C<sup>13</sup> (DMSO-d<sub>6</sub>, 15 MHz,  $\delta$  ppm): 14.0 (CH<sub>3</sub>); 18.3 (CH<sub>3</sub>); 19.1 (CH<sub>3</sub>); 19.4 (CH<sub>3</sub>); 53.2 (CH); 60.2 (CH<sub>2</sub>); 105.6 (C); 113.3 (C-arom); 114.9 (C-arom); 117.1 (C-arom); 129.8 (C-arom); 136.5 (C-arom); 136.7 (C-arom); 138.1 (C-arom); 144.3 (C-arom); 146.3 (C); 157.7 (C-arom); 165.4 (C); 177.4 (C). HRMS/MS ( $m/z$ ): calcd. C<sub>22</sub>H<sub>24</sub>N<sub>2</sub>O<sub>3</sub>S [M + H]<sup>+</sup>: 397.15803, found 397.15800.

## Molecular docking

The molecules 19a–k and 20a–k were first drawn and minimized on a CORINA webserver<sup>45</sup> and were then minimized using the semi-empiric method PM6 in Spartan 14 V.1.1.4 (ref. 46) in order to obtain tridimensional structures with bond lengths and chemically appropriate angles.

Molecular docking simulations were accomplished using the crystallographic structure of kinesin Eg5 bound with monastrol (PDBID: 1X88) using GOLD 5.0.3 from the Cambridge Crystallographic Data Center (CCDC).<sup>47</sup> The molecular docking procedure began with protein preparation using the protein preparation wizard from Schrödinger Maestro suite.<sup>48,49</sup> The protein preparation was performed in Maestro *via*: (a) insertion of hydrogen atoms, (b) assignment of bond orders, (c) filling of missing side chains using Prime, (d) deletion of water molecules, (e) deletion of the protein chain B, (f) assignment of ligand protonation states and metal binding states at pH 7.0  $\pm$  2.0 using Epik, (g) protonation of amino acid residues at pH 7.0 using PropKA, and (h) restrained minimization of all atoms of the crystal structure using the OPLS2005 force field with a convergence of heavy atoms of 0.30 Å.

Before starting the virtual screening procedure using the designed molecules, the docking parameters (*e.g.* grid size and position) were validated according to the re-docking and cross-docking results. Re-docking and cross-docking runs were evaluated through comparison of the docked poses with the respective crystallographic ligands, in accordance with criteria previously reported by Caroli and coworkers.<sup>50</sup> The cross-docking method consisted of docking several different ligands extracted from other crystallographic structures of kinesin Eg5 (Table S8 in the ESI†) into the binding site of PDB ID 1X88. The superposition of the crystallographic

structures was achieved by UCSF Chimera,<sup>51</sup> and the RMSD analyses were performed using Discovery Studio Visualizer 16.1.<sup>52</sup>

The virtual screening procedure of GOLD involved extraction of the bound ligands and of the co-factors for later comparison. The crystallographic ligands were included with the designed DHPMs for rank comparison. The algorithms were applied with 100% efficiency and the search efficiency flexibility was set to 100% (flexible – default). The grid region was set over the ligand (monastrol) with a 6 Å radius sphere. The genetic algorithm (GA) runs were set at 10 runs per ligand; the best solutions were saved for each ligand, and all 10 solutions were analyzed. The docking poses were then ranked using the dimensionless scoring function GoldScore. The score scale indicates how good a pose is; the higher the score, the better the docking result is likely to be. The best two compounds were selected through visual inspection of their poses and their respective ranking positions. The best molecules were analyzed with their counterpart analogues in accordance with their interactions with the kinesin binding site using DSV 16.1 (ref. 52) and the Ligand Explorer Java module.<sup>53</sup>

The binding affinities were predicted using the X-Score. The X-Score is an empirical score function that correlates the binding affinity with the dissociate constant of a protein–ligand complex ( $-\log K_d$ ). The X-Score values are positive numbers ranging from 3.0 to 9.0, predicting a milli-molar to a nano-molar affinity.<sup>54</sup>

### *In vitro* activity against glioma cells

**Maintenance of cell lines.** The human U138 and rat C6 glioma cell lines were obtained from the American Type Culture Collection (ATCC) (Rockville, MD, USA). The cells were grown and maintained in Dulbecco's modified Eagle's medium (DMEM) containing antibiotics (0.5 U mL<sup>-1</sup> penicillin/streptomycin) and supplemented with 15% and 5% (v/v) fetal bovine serum (FBS), respectively (all from Gibco BRL, Carlsbad, CA, USA). The cells were maintained at a temperature of 37 °C, a minimum relative humidity of 95%, and an atmosphere of 5% CO<sub>2</sub> in the air.

**Assessment of glioma cell viability.** For the [3-(4,5-dimethylthiazol-2-yl)-5-(3-carboxymethoxyphenyl)-2-(4-sulphophenyl)-2H-tetrazolium] (MTS) assay, U138 and C6 glioma cells were seeded in 96-well plates and allowed to grow to semi-confluence. The cells were treated with 5, 10, 25, 50 and 100 µM of monastrol or **19e**, **20e**, **19h** or **20h** for 24 h. At the end of the treatment, 20 µL of MTS (5 mg mL<sup>-1</sup>) reagent was added to each well for 2 h. At the end of the incubation time, the absorbance was read at 490 nm.

**Cell-cycle analysis.** The cells were plated in 6-well plates; after reaching semi-confluence, they were treated with 50 µM **20e** or **20h** or 100 µM monastrol 1 (positive control) for 24 h. At the end of the treatment, the cell medium was removed and the cells were washed twice with PBS (pH 7.4), harvested, centrifuged, and suspended with 400 µL staining solution

[Tris-HCl 0.5 mM (pH 7.6); 3.5 mM trisodium citrate; 0.1% (v/v) NP40; 100 µg mL<sup>-1</sup> RNase; 50 µg mL<sup>-1</sup> propidium iodide (PI)] at a density of 10<sup>6</sup> cells per ml. After 15 min, data were collected using a flow cytometer (FACS Calibur cytometric system; BD Bioscience, Mountain View, CA, USA) and analyzed by FLOWJO® software.

**Annexin V/PI assay.** Apoptotic cells were quantified using an annexinV-fluorescein isothiocyanate–PI (annexinV-FITC–PI) double staining kit in accordance with the manufacturer's instructions (BD Biosciences, San Diego, CA, USA). The cells were plated in 6-well plates and treated with 50 µM **20e** or **20h** or 100 µM monastrol 1 for 48 h. At the end of the treatment, the cells were washed twice with cold PBS (pH 7.4) and counted. Following this, 10<sup>5</sup> cells were suspended in binding buffer containing FITC-conjugated annexin V and PI. The samples were then agitated and incubated for 15 minutes at room temperature in the dark. Apoptotic and necrotic cells were quantified using a dual-color flow cytometric technique on a FACSCalibur cytometric system (FACSCalibur; BD Bioscience, Mountain View, CA, USA). The obtained data were analyzed with LOWJO® software (Tree Star, INC Ashland, OR, USA). The cells were classified as follows: live, annexin<sup>-</sup>/PI<sup>-</sup>; early apoptotic, annexin<sup>+</sup>/PI<sup>-</sup>; late apoptotic, annexin<sup>+</sup>/PI<sup>+</sup>, and necrotic, annexin<sup>-</sup>/PI<sup>+</sup>.

**Immunocytochemistry.** To access the formation of monopolar spindles resulting from Eg5 inhibition, U138 and C6 glioma cells were left to adhere to confocal 4-well plates for 48 hours before treatment. Following this, the U138 cells were treated with 200 µM monastrol or 150 µM of **20e** or **20h**, while the C6 cells were treated with 100 µM monastrol or 50 µM of **20e** or **20h** for 24 hours. After treatment, the cells were washed with PBS, fixed, and then incubated with anti-alpha-tubulin (ab52866, Abcam Ltd., Cambridge, UK) for 90 minutes, followed by incubation with fluorescein (FITC)-conjugated goat anti-rabbit (Invitrogen, Life Technologies Ltd, Paisley, UK) secondary antibody for one hour. The cells were washed with PBS and incubated with Hoechst, a nuclear marker. Imaging was performed on an Olympus FluoView™ 1000 197 confocal microscope equipped with solid state lasers of 405, 198 473, 559, and 635 nm (Centro de Microscopia Eletrônica da Universidade Federal do Rio Grande do Sul).

**Statistical analysis.** Data were analyzed for statistical significance by one-way analysis of variance (ANOVA) followed by post-hoc tests for multiple comparisons (Tukey test) using GraphPad Prism Software® (GraphPad Software, INC, La Jolla, CA, USA). Data are expressed as the mean ± S.E.M.

### Toxicity assays on *Caenorhabditis elegans*

The nematode strain used was N2 (wild type), originally obtained from the *Caenorhabditis* Genetics Center (University of Minnesota, Twin Cities, MN, USA); the worms were maintained on nematode growth medium (NGM) plates seeded with *Escherichia coli* OP50 at 20 °C. Synchronization of *C. elegans* cultures at the first larval stage (L1) was achieved by washing the gravid nematodes from the plates



into centrifuge tubes, which were lysed with a bleaching mixture (1% NaOCl; 0.25 M NaOH), followed by flotation on a 30% (m/v) sucrose solution to separate the eggs from the dissolved worms and bacterial debris. The eggs were washed with M9 buffer (0.02 M  $\text{KH}_2\text{PO}_4$ , 0.04 M  $\text{Na}_2\text{HPO}_4$ , 0.08 M NaCl, and 0.001 M  $\text{MgSO}_4$ ) and allowed to hatch overnight in NGM agar plates without bacteria. The toxicities of monastrol **1**, **20e** and **20h** to *C. elegans* were then evaluated through the following toxicological endpoint: lethal dose 50% ( $\text{LC}_{50}$ ).  $\text{LC}_{50}$  was determined after acute exposure of the *C. elegans* L1 larva to five doses of monastrol **1**, **20e** and **20h**, ranging from 6.25 to 200 mM. Accordingly, synchronized L1 larvae (2,500 worms per dose) were treated at 20 °C for 30 minutes by constant agitation in a rotator with each dose of the compounds. The worms were then washed three times with M9 buffer and placed on OP50-seeded NGM plates (60 × 10 mm) to determine the number of surviving organisms (24 hours post-exposure). The dose-response curves were obtained by plotting the numbers of surviving worms, and the  $\text{LC}_{50}$  values were calculated from those curves.

## Conflicts of interest

The authors declare no competing interest.

## Acknowledgements

The authors are thankful to CNPq/MCT, INCT-if (Instituto Nacional de Ciência e Tecnologia para Inovação Farmacêutica), ICNT- DCEN (Instituto Nacional de Ciência e Tecnologia: Doenças Cerebrais, Excitotoxicidade e Neuroproteção), FINEP, IQ-UFRGS and to Programa de Pós-graduação em Ciências-Bioquímica da Universidade Federal do Paraná. The authors are grateful to CNPq and CAPES for their scholarships.

## References

- J. A. Schwartzbaum, J. L. Fisher, K. D. Aldape and M. Wrensch, *Nat. Clin. Pract. Neurol.*, 2006, 2, 494–503.
- H. Ohgaki and P. Kleihues, *Acta Neuropathol.*, 2005, 109, 93–108.
- W. Zhu, L. Zhou, J.-Q. Qian, T.-Z. Qiu, Y.-Q. Shu and P. Liu, *World J. Clin. Oncol.*, 2014, 5, 19.
- Y. Yi, I. Y. Hsieh, X. Huang, J. Li and W. Zhao, *Front. Pharmacol.*, 2016, 7, 477.
- C. P. Haar, P. Hebbbar, G. C. Wallace, A. Das, W. A. Vandergrift, J. A. Smith, P. Giglio, S. J. Patel, S. K. Ray and N. L. Banik, *Neurochem. Res.*, 2012, 37, 1192–1200.
- O. Valiron, N. Caudron and D. Job, *Cell. Mol. Life Sci.*, 2001, 58, 2069–2084.
- A. Canta, A. Chiorazzi and G. Cavaletti, *Curr. Med. Chem.*, 2009, 16, 1315–1324.
- S. Ding, Z. Zhao, D. Sun, F. Wu, D. Bi, J. Lu, N. Xing, L. Sun, H. Wu and K. Ding, *Tumor Biol.*, 2014, 35, 7659–7668.
- D. Huszar, M.-E. Theoclitou, J. Skolnik and R. Herbst, *Cancer Metastasis Rev.*, 2009, 28, 197–208.
- S. M. Myers and I. Collins, *Future Med. Chem.*, 2016, 8, 463–489.
- Y. Duan, D. Huo, J. Gao, H. Wu, Z. Ye, Z. Liu, K. Zhang, L. Shan, X. Zhou and Y. Wang, *Nat. Commun.*, 2016, 7, 1–12.
- M. Lu, H. Zhu, X. Wang, D. Zhang, L. Xiong, L. Xu and Y. You, *Pathology*, 2016, 48, 214–218.
- L. Liu, X. Liu, M. Mare, A. S. Dumont, H. Zhang, D. Yan and Z. Xiong, *J. Neuro-Oncol.*, 2016, 126, 77–80.
- M. D. Wissing, E. S. De Morree, V. O. Dezentje, J. T. Buijs, R. R. De Krijger, V. T. Smit, W. M. Van Weerden, H. Gelderblom and G. Van Der Pluijm, *Oncotarget*, 2014, 5, 7357.
- L. Sun, J. Lu, Z. Niu, K. Ding, D. Bi, S. Liu, J. Li, F. Wu, H. Zhang and Z. Zhao, *PLoS One*, 2015, 10, e0144484.
- H. B. El-Nassan, *Eur. J. Med. Chem.*, 2013, 62, 614–631.
- T. U. Mayer, T. M. Kapoor, S. J. Haggarty, R. W. King, S. L. Schreiber and T. J. Mitchison, *Science*, 1999, 286, 971–974.
- Z. Maliga, T. M. Kapoor and T. J. Mitchison, *Chem. Biol.*, 2002, 9, 989–996.
- M. E. Welsch, S. A. Snyder and B. R. Stockwell, *Curr. Opin. Chem. Biol.*, 2010, 14, 347–361.
- L. H. S. Matos, F. T. Masson, L. A. Simeoni and M. Homem-de-Mello, *Eur. J. Med. Chem.*, 2017, 143, 1779–1789.
- M. Gartner, N. Sunder-Plassmann, J. Seiler, M. Utz, I. Vernos, T. Surrey and A. Giannis, *ChemBioChem*, 2005, 6, 1173–1177.
- H. Prokopcová, D. Dallinger, G. Uray, H. Y. K. Kaan, V. Ulaganathan, F. Kozielski, C. Laggner and C. O. Kappe, *ChemMedChem*, 2010, 5, 1760–1769.
- R. F. Canto, A. Bernardi, A. M. O. Battastini, D. Russowsky and V. L. Eifler-Lima, *J. Braz. Chem. Soc.*, 2011, 22, 1379–1388.
- F. Figueiro, F. B. Mendes, P. F. Corbelini, F. Janarelli, E. H. F. Jandrey, D. Russowsky, V. L. Eifler-Lima and A. M. O. Battastini, *Anticancer Res.*, 2014, 34, 1837–1842.
- C. S. Stuepp, F. Figueiró, F. B. Mendes, E. Braganhol, A. Bernardi, R. L. Frozza, C. G. Salbego, R. F. S. Canto, D. Russowsky, V. L. Eifler-Lima and A. M. O. Battastini, *Anticancer Res.*, 2013, 33, 4463–4468.
- L. M. Ramos, B. C. Guido, C. C. Nobrega, J. R. Corrêa, R. G. Silva, H. C. de Oliveira, A. F. Gomes, F. C. Gozzo and B. A. Neto, *Chem. – Eur. J.*, 2013, 19, 4156–4168.
- F. A. R. Barbosa, R. F. S. Canto, S. Saba, J. Rafique and A. L. Braga, *Bioorg. Med. Chem.*, 2016, 24, 5762–5770.
- S. Putatunda, S. Chakraborty, S. Ghosh, P. Nandi, S. Chakraborty, P. C. Sen and A. Chakraborty, *Eur. J. Med. Chem.*, 2012, 54, 223–231.
- K. Singh, D. Arora, E. Poremsky, J. Lowery and R. S. Moreland, *Eur. J. Med. Chem.*, 2009, 44, 1997–2001.
- E. N. Ostapchuk, A. S. Plaskon, O. O. Grygorenko, A. A. Tolmachev and S. V. Ryabukhin, *J. Heterocyclic Chem.*, 2013, 50, 1299–1303.
- S. V. Ryabukhin, A. S. Plaskon, E. N. Ostapchuk, D. M. Volochnyuk and A. A. Tolmachev, *Synthesis*, 2007, 417–427.
- M. Strocchia, S. Terracciano, M. G. Chini, A. Vassallo, M. C. Vaccaro, F. Dal Piaz, A. Leone, R. Riccio, I. Bruno and G. Bifulco, *Chem. Commun.*, 2015, 51, 3850–3853.

- 33 A. Stadler and C. O. Kappe, *J. Comb. Chem.*, 2001, 3, 624–630.
- 34 P. Zalavadiya, R. Ghetiya, B. Dodiya, P. Vekariya and H. Joshi, *J. Heterocyclic Chem.*, 2013, 50, 973–978.
- 35 W.-J. Li, S. Liu, P. He and M.-W. Ding, *Tetrahedron*, 2010, 66, 8151–8159.
- 36 A. Dandia, M. Saha and H. Taneja, *J. Fluorine Chem.*, 1998, 90, 17–21.
- 37 M. Kidwai, S. Kukreja, S. Rastogi and K. Singhal, *Lett. Org. Chem.*, 2007, 4, 357–361.
- 38 J. A. Good, F. Wang, O. Rath, H. Y. K. Kaan, S. K. Talapatra, D. Podgórski, S. P. MacKay and F. Kozielski, *J. Med. Chem.*, 2013, 56, 1878–1893.
- 39 F. Wang, J. A. Good, O. Rath, H. Y. K. Kaan, O. B. Sutcliffe, S. P. Mackay and F. Kozielski, *J. Med. Chem.*, 2012, 55, 1511–1525.
- 40 V. Zoete, A. Grosdidier and O. Michielin, *J. Cell. Mol. Med.*, 2009, 13, 238–248.
- 41 M. L. Verdonk, P. N. Mortenson, R. J. Hall, M. J. Hartshorn and C. W. Murray, *J. Chem. Inf. Model.*, 2008, 48, 2214–2225.
- 42 H. Y. K. Kaan, V. Ulaganathan, O. Rath, H. Prokopcová, D. Dallinger, C. O. Kappe and F. Kozielski, *J. Med. Chem.*, 2010, 53, 5676–5683.
- 43 W. G. Salgueiro, M. C. Xavier, L. F. Duarte, D. F. Camara, D. A. Fagundez, A. T. Soares, G. Perin, D. Alves and D. S. Avila, *Eur. J. Med. Chem.*, 2014, 75, 448–459.
- 44 W. G. Salgueiro, B. S. Goldani, T. V. Peres, A. Miranda-Vizuete, M. Aschner, J. B. T. da Rocha, D. Alves and D. S. Avila, *Free Radical Biol. Med.*, 2017, 110, 133–141.
- 45 J. Sadowski, J. Gasteiger and G. Klebe, *J. Chem. Inf. Comput. Sci.*, 1994, 34, 1000–1008.
- 46 *Spartan, Ver. 14.1.1.4*, Wavefunction. Inc., Irvine, CA, 2014.
- 47 G. Jones, P. Willett, R. C. Glen, A. R. Leach and R. Taylor, *J. Mol. Biol.*, 1997, 267, 727–748.
- 48 R. A. Friesner, J. L. Banks, R. B. Murphy, T. A. Halgren, J. J. Klicic, D. T. Mainz, M. P. Repasky, E. H. Knoll, M. Shelley, J. K. Perry, D. E. Shaw, P. Francis and P. S. Shenkin, *J. Med. Chem.*, 2004, 47, 1739–1749.
- 49 T. A. Halgren, R. B. Murphy, R. A. Friesner, H. S. Beard, L. L. Frye, W. T. Pollard and J. L. Banks, *J. Med. Chem.*, 2004, 47, 1750–1759.
- 50 A. Caroli, F. Ballante, R. B. Wickersham, F. Corelli and R. Ragno, *J. Chem. Inf. Model.*, 2014, 54, 970–977.
- 51 E. F. Pettersen, T. D. Goddard, C. C. Huang, G. S. Couch, D. M. Greenblatt, E. C. Meng and T. E. Ferrin, *J. Comput. Chem.*, 2004, 25, 1605–1612.
- 52 *Spartan, Ver. 14.1.1.4*, Wavefunction. Inc., Irvine, CA, 2014.
- 53 J. L. Moreland, A. Gramada, O. V. Buzko, Q. Zhang and P. E. Bourne, *BMC Bioinf.*, 2005, 6, 21.
- 54 R. Wang, L. Lai and S. Wang, *J. Comput.-Aided Mol. Des.*, 2002, 16, 11–26.